

Graph Artificial Intelligence for Quantifying Compatibility Mechanisms in Traditional Chinese Medicine

Jingqi Zeng¹, Xiaobin Jia^{1,2*}

¹School of Traditional Chinese Pharmacy, China Pharmaceutical University; Nanjing, China.

²State Key Laboratory of Natural Medicines, China Pharmaceutical University; Nanjing, China.

*Corresponding author. Email: ji Xiaobin2015@163.com

Abstract: Traditional Chinese Medicine (TCM) involves complex compatibility mechanisms characterized by multi-component and multi-target interactions, which are challenging to quantify. To address this challenge, we applied graph artificial intelligence to develop a TCM multi-dimensional knowledge graph that bridges traditional TCM theory and modern biomedical science (<https://zenodo.org/records/13763953>). Using feature engineering and embedding, we processed key TCM terminology and Chinese herbal pieces (CHP), introducing medicinal properties as virtual nodes and employing graph neural networks with attention mechanisms to model and analyze 6,080 Chinese herbal formulas (CHF). Our method quantitatively assessed the roles of CHP within CHF and was validated using 215 CHF designed for COVID-19 management. With interpretable models, open-source data, and code (<https://github.com/ZENGJingqi/GraphAI-for-TCM>), this study provides robust tools for advancing TCM theory and drug discovery.

Keywords

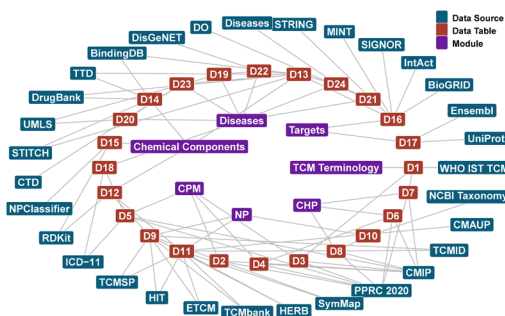
Traditional Chinese Medicine; Graph Artificial Intelligence; Knowledge Graph; Compatibility Mechanism; Herbal Synergy; Graph Neural Networks; COVID-19

One-Sentence Summary

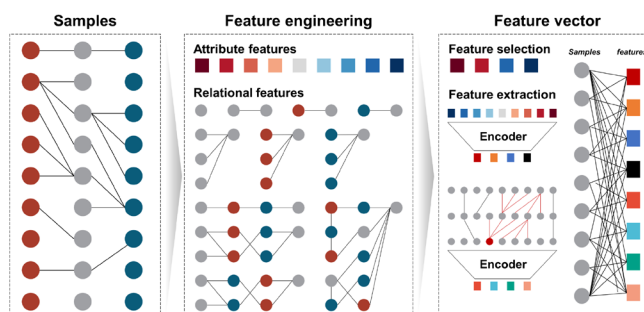
We quantified Traditional Chinese Medicine compatibility using graph artificial intelligence, enabling interpretable insights into herbal synergy.

Graphic Abstract

① Construct a Traditional Chinese Medicine (TCM) Multi-dimensional Knowledge Graph



② Engineer and embed attribute and relational features of TCM terminology, e.g., Chinese herbal pieces (CHP), medicinal properties

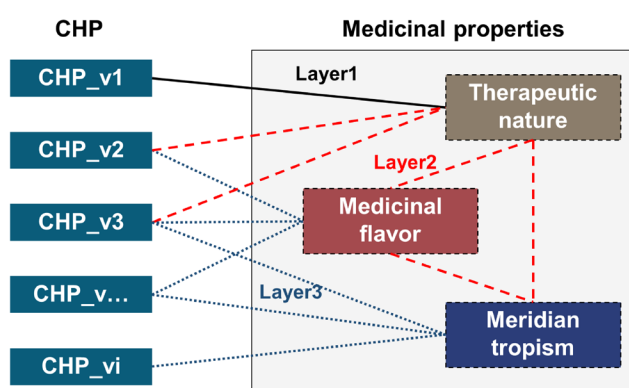


④ Quantitatively evaluate the compatibility mechanisms of CHP within CHF by utilizing node attention weights

Table showing attention weights for Huashi Baidu decoction. The table lists Source (CHP IDs) and Target (CHP IDs) with attention weights for each pair.

Source	CHP00299	CHP00303	CHP00316	CHP00513	CHP01118	CHP01308	CHP01771	CHP02346	CHP03635	CHP04173	CHP04195	CHP06090	CHP06191
CHP06191	0.016	0.016	0.025	0.012	0.017	0.014	0.024	0.020	0.020	0.020	0.020	0.020	0.017
CHP06090	0.011	0.011	0.017	0.008	0.011	0.009	0.015	0.013	0.013	0.013	0.013	0.013	0.015
CHP04795	0.008	0.008	0.012	0.006	0.008	0.007	0.011	0.010	0.009	0.009	0.009	0.017	0.008
CHP04173	0.033	0.033	0.052	0.025	0.034	0.028	0.048	0.041	0.041	0.040	0.049	0.052	0.034
CHP03635	0.019	0.019	0.029	0.015	0.020	0.016	0.027	0.024	0.023	0.032	0.023	0.030	0.019
CHP02546	0.007	0.007	0.011	0.005	0.007	0.006	0.010	0.009	0.011	0.008	0.009	0.011	0.007
CHP01771	0.006	0.006	0.009	0.005	0.006	0.005	0.009	0.010	0.007	0.007	0.007	0.009	0.006
CHP01717	0.067	0.068	0.101	0.051	0.068	0.097	0.144	0.082	0.080	0.079	0.080	0.102	0.068
CHP01508	0.008	0.008	0.012	0.006	0.008	0.009	0.011	0.010	0.009	0.009	0.009	0.012	0.008
CHP01118	0.009	0.009	0.014	0.007	0.013	0.008	0.013	0.011	0.011	0.011	0.011	0.014	0.009
CHP00513	0.008	0.008	0.013	0.008	0.008	0.007	0.012	0.010	0.010	0.010	0.010	0.013	0.008
CHP00316	0.009	0.009	0.022	0.007	0.010	0.008	0.013	0.011	0.011	0.011	0.011	0.014	0.010
CHP00303	0.011	0.015	0.017	0.008	0.011	0.009	0.015	0.013	0.013	0.013	0.013	0.017	0.011
CHP00209	0.007	0.006	0.009	0.004	0.006	0.005	0.008	0.007	0.007	0.007	0.007	0.009	0.006
CHP00299													
CHP00303													
CHP00316													
CHP00513													
CHP01118													
CHP01308													
CHP01771													
CHP02346													
CHP03635													
CHP04173													
CHP04195													
CHP06090													
CHP06191													

③ Incorporate medicinal properties as virtual nodes with attention propagation for Chinese herbal formulas (CHF) graph encoding



Highlights

- 1) Developed a TCM multi-dimensional knowledge graph integrating traditional concepts with modern biomedical data.
- 2) Introduced virtual nodes in graph encoding to enhance compatibility modeling in Chinese herbal formulas.
- 3) Released open-source data, models, and code for advancing TCM research and applications.
- 4) Quantified key roles of Chinese herbal pieces and herb pairs in COVID-19 management.
- 5) Identified Radix Astragali as a central herb in COVID-19 management with enriched targets in three KEGG pathways.

Introduction

Traditional Chinese Medicine (TCM) emphasizes a holistic perspective and dynamic balance, focusing on the comprehensive evaluation of an individual’s constitution, disease state, and the interplay among various physiological systems. Through the rational compatibility of herbal medicines, TCM achieves synergistic effects and toxicity reduction [1]. This core principle has demonstrated significant advantages in treating complex diseases. For example, Lianhua Qingwen Capsules have shown remarkable efficacy in alleviating symptoms and reducing hospitalization time for COVID-19 patients [2, 3]. Additionally, PHY906, developed by Yale University based on the traditional Huangqin Decoction, has improved colorectal cancer treatment outcomes as a chemotherapy adjuvant [4].

In recent years, the rapid development of artificial intelligence (AI) has introduced novel opportunities for investigating the complex mechanisms underlying TCM [5, 6]. AI’s exceptional data processing capabilities, particularly in multi-dimensional data analysis and complex relationship modeling, are transforming traditional medicine from experience-driven to data-driven paradigms [7-9]. Notably, Graph Artificial Intelligence (GraphAI) offers a unique toolkit for exploring complex network-structured data by integrating knowledge graphs, graph computation, and graph neural networks (GNNs) [10, 11]. The core challenges of TCM compatibility—complex interactions involving multiple components, targets, and pathways—align closely with GraphAI’s strengths in handling intricate relationships [12-14].

However, existing data-driven approaches in TCM research face three major challenges. First, the quantification and analysis of intricate herbal interactions remain insufficient, with existing models lacking interpretability to provide clear mechanistic insights. Second, the design of current models often fails to incorporate core TCM theories, limiting the alignment between theoretical foundations and computational frameworks. Lastly, the absence of high-quality, multi-dimensional, and openly shared TCM datasets constrains interdisciplinary collaboration and innovation.

To address these challenges, this study proposes a method for quantifying TCM compatibility mechanisms based on GraphAI, deeply integrating TCM theories with modern AI technologies to achieve the digitization and quantification of TCM compatibility. We developed a TCM Multi-dimensional Knowledge Graph (TCM-MKG), encompassing multi-layered information spanning traditional TCM theories and modern biomedical science. This graph integrates TCM compatibility relationships, chemical compositions, target interactions, biological networks, and disease-diagnosis knowledge, offering comprehensive multi-dimensional data support for elucidating TCM’s complex systems.

Using the TCM-MKG, we modeled Chinese herbal pieces (CHP) as units, incorporating medicinal properties and diagnostic theories. By leveraging graph neural networks with attention mechanisms, we analyzed 6,080 Chinese herbal formulas (CHF) and constructed highly interpretable models to quantify the compatibility roles of CHP within CHF. This method unveiled synergistic effects and compatibility mechanisms among herbs and was validated on 215 CHF used in China’s COVID-19 management from 2019 to 2021. The results demonstrate the method’s efficacy in advancing TCM theory modernization, data-driven research, and drug discovery, providing new pathways for disciplinary progress and enhanced healthcare services.

Results

Data structure and compound-target discovery in the TCM multi-dimensional knowledge graph

Data-driven research in TCM has long faced challenges in data standardization and cross-disciplinary interoperability, limiting the systematic integration of traditional TCM theories with modern biomedical knowledge. To address these issues, we constructed the TCM-MKG, which integrates seven core modules: TCM terminology, Chinese patent medicines (CPM), CHP, natural products (NP), chemical compounds, targets, and diseases (Figure 1A). The data were sourced from 31 authoritative databases and standardized through semantic integration, resulting in a multi-layered knowledge framework organized into 24 primary data tables (detailed in Data S1). This provides systematic support for interdisciplinary research.

The TCM terminology module comprises 1,810 standardized terms, forming the semantic foundation for etiology, pathogenesis, and therapeutic principles. These terms are interconnected with CPM, disease, and target modules, serving as the semantic core of the knowledge graph. The CPM module documents the basic information of 8,977 formulas and systematically organizes their compatibility structures through 11,185 records linking formulas to TCM terms and 74,084 records linking formulas to CHP. Additionally, 69,431 records mapping CPM formulas to ICD-11 enable data interoperability between traditional Chinese and modern Western medicine. Analysis revealed that CPM formulas contain an average of eight CHP (Figure 1B), highlighting the multi-herbal compatibility typical of TCM. The average dose ratio among CHP was 0.11 (Figure 1C), reflecting the uneven distribution of herbal quantities.

The CHP module details 6,207 CHP, 23,517 medicinal property records, and 226,589 associations between CHP and chemical compounds, comprehensively describing the pharmacological and molecular basis of CHP. The NP module includes 4,810 natural products, linked to the chemical compound module through 426,305 associations. While these modules provide essential data, early compound-target association data showed limited coverage. Of the 123,647 documented compounds, 62,830 were associated with CHP or their linked NPs, but only 12.1% had defined target information (Figure 1D), posing a bottleneck in studying TCM molecular mechanisms.

To address this core issue, we proposed a neighbor-diffusion-based compound-target prediction strategy. Using GNN models, we systematically expanded potential target data for TCM compounds. Molecular structures of TCM compounds were parsed into molecular graphs using RDKit, representing atoms and chemical bonds as nodes and edges, respectively. We employed three embedding methods—Graph Convolutional Network (GCN), Graph Attention Network (GAT), and Graph Autoencoder (GAE)—along with 197 molecular descriptors and 2,048-bit Morgan fingerprints to comprehensively encode the physicochemical properties and structural information of the molecules. All high-dimensional features were reduced using Uniform Manifold Approximation and Projection (UMAP), preserving both local and global data structures (Figure 1E). Based on these reduced features, we calculated the distance between TCM compounds and their nearest neighbor molecules with known targets, generating candidate compound-target pairs using a neighbor-diffusion approach. This method produced 7,260,578 extended target associations (Figure 1F), validated using the PSICHIC model (<https://github.com/huankoh/PSICHIC>) [15]. Using the PSICHIC model's binding affinity threshold of 5.0, we filtered high-confidence compound-target associations to ensure prediction reliability.

We analyzed binding affinity distributions across three data types: “TCM diffused targets” 7,260,578 samples, “High fidelity targets,” 283,793 samples, including 10,000 randomly selected non-TCM compound samples for control, and “Recorded TCM targets” 343,373 samples. Results showed that “TCM diffused targets” matched the distribution pattern of “High fidelity targets” in the high-affinity range (>5.0), whereas “Recorded TCM targets” exhibited lower affinities, validating the effectiveness of the neighbor-diffusion strategy. Further affinity threshold analysis revealed a significant increase in coverage (Figures 1G–I). At a threshold of 5.0, InChIKey coverage reached 99.86%, with compounds increasing from 7,631 to 62,744. EntrezID coverage rose to 99.0%, with targets increasing from 13,781 to 14,370. Compound-target associations expanded from 343,373 to 6,526,940, an 18-fold increase.

To validate the performance of different feature representation methods and evaluate the influence of molecular weight and target sequence length on binding affinity prediction, we conducted in-depth analyses (Figures S1 and S2, Supporting Information). Results further supported the reliability and applicability of the neighbor-diffusion method in expanding target data. This study significantly enhanced the coverage of TCM compound-target associations, laying a robust data foundation for exploring TCM mechanisms and compatibility principles. All extended data have been made publicly available (dataset: <https://zenodo.org/records/13763953>).

Feature engineering and embedding of Chinese herbal pieces

The multi-dimensional characteristics of CHP introduce complexity and diversity into pharmacological research. To comprehensively represent the origin, medicinal properties, efficacy, and compatibility of CHP, this study proposed a multi-modal feature integration method. By combining feature engineering with vector embedding techniques, we generated unified feature vector representations. This approach, inspired by strategies for multi-modal feature integration and multi-task learning [16], provides a robust data foundation for in-depth analysis of CHP’ roles in complex compatibility mechanisms.

Figure 2 illustrates the encoding process of multi-source CHP features and their dimensionality-reduction visualizations. For origin attribute features, we extracted 10 principal components using phylogenetic tree genetic distances and principal component analysis (PCA). These were combined with dummy variables for the Plantae, Animalia, Fungi, Algae, and Mineralia kingdoms to generate a 15-dimensional origin feature vector. Supporting Information Figure S3 details the extraction and phylogenetic structure of origin features. Additionally, medicinal property, efficacy, and compatibility features, representing relational attributes, were encoded using a Word2Vec model, generating 15-dimensional medicinal property vectors, 30-dimensional efficacy vectors, and 30-dimensional compatibility vectors. To ensure scale consistency across multi-source features, all features were standardized before fusion (Figure 2A).

Dimensionality-reduction analysis revealed distinct characteristics for each feature type under UMAP projections (Figures 2B–E). Origin features (Figure 2B) exhibited clear hierarchical structures, with CHP from different origin categories forming well-defined clusters, effectively reflecting biological source attributes. Medicinal property features (Figure 2C) showed moderate patterns in encoding flavor and nature information but had weaker category distinctions. Compatibility features (Figure 2D) captured synergistic relationships of CHP in formulas, though category boundaries were less pronounced. Efficacy features (Figure 2E) excelled in revealing

relationships between CHP and their therapeutic applications, showing clear clustering and underscoring their strength in representing functional information.

To enhance the expressive power of multi-dimensional features, medicinal property, efficacy, and compatibility features were combined into a composite relational feature (Figure 2F). This composite representation significantly improved category separation, with CHP from different origin categories exhibiting clearer distributions in the dimensionality-reduction space. This validated the effectiveness of multi-modal feature integration. Building on this, origin features were fused with composite relational features to generate a 90-dimensional comprehensive feature vector (Figure 2G). UMAP projections of these integrated features demonstrated stronger structural organization and more distinct category boundaries, further confirming the utility of the multi-modal feature fusion strategy for characterizing complex attributes.

To compare the adaptability of different dimensionality-reduction methods, we also applied t-SNE to all features (Figure 2H). The results showed consistency with UMAP projections, demonstrating excellent category separation and further supporting the robustness and adaptability of the multi-modal feature integration method.

By encoding and integrating multi-modal features, this study effectively unified the origin, medicinal properties, efficacy, and compatibility attributes of CHP into a comprehensive and efficient feature vector. This feature representation method establishes a technical foundation for data-driven characterization of CHP, while providing critical support for exploring TCM compatibility mechanisms and constructing formula models.

Encoding and classification of medicinal properties and diagnostic terminologies in TCM

The medicinal properties of CHP are fundamental for understanding their efficacy and compatibility principles. To systematically characterize relationships among these properties, this study standardized attributes including therapeutic nature, medicinal flavor, and meridian tropism, constructing an undirected network-based medicinal property knowledge graph. Heatmap analysis (Figure 3A) visualized the interaction strength between these attributes, with color intensity intuitively reflecting their relationships. The optimized medicinal property network (Figure 3B) was refined using the ForceAtlas2 algorithm, achieving a more even spatial distribution of nodes and clearer logical relationships. Community detection using the Louvain method divided the network into functional modules, significantly enhancing intra-module node connectivity.

Diagnostic terminologies, an integral part of the TCM theoretical framework, are essential for systematic studies of etiology, pathogenesis, and therapeutic principles. Using the Node2Vec algorithm, we constructed a 32-dimensional graph model embedding diagnostic terminologies into a high-dimensional space to form a structured graph network (Figure 3C). UMAP dimensionality reduction (Figure 3D) revealed significant clustering of diagnostic terminologies in two-dimensional space, providing clear bases for classification and clustering.

Hierarchical clustering analysis based on the 32-dimensional feature vectors divided diagnostic terminologies into six TCM etiological categories (Figure 3E). The proportional distributions of etiology, pathogenesis, treatment principles, and therapeutic methods within each category (Figure 3F) highlighted distinct diagnostic characteristics. From these clusters, we identified primary features, detailed in the supporting material: metabolic and circulatory imbalances within the body

(Figure S4); organ aging and immune deficiency (Figure S5); influences of lifestyle and environmental conditions (Figure S6); physical and mental stress and external stimuli (Figure S7); internal pathological changes and infectious factors (Figure S8); dry dampness and harmonize the stomach (Figure S9). Due to the limited sample size of Category 6, subsequent analyses focused on the five TCM etiological categories.

To further explore the characteristics of diagnostic terminology categories, we quantified node importance using ten centrality metrics (results in Supporting Information Figure S10). Core diagnostic features for each category were extracted by analyzing their central feature vectors, culminating in the construction of a diagnostic feature matrix for five major TCM disease types (Figure 3G). This matrix systematically presents the specific distributions of etiology, pathogenesis, and therapeutic principles. It not only clarifies the core features of each disease type but also provides essential data support for the quantitative and modernized analysis of TCM diagnostic terminologies.

Graph encoding and attention mechanisms for Chinese herbal formulas

Using a graph encoding method based on virtual nodes, this study constructed a multi-dimensional relational network for CHF and systematically analyzed their complex compatibility relationships with three GNN models: Graph Transformer Network (GTN), Hypergraph Neural Network (HGNN), and Graph Attention Network (GAT) (Figure 4A). In the constructed graph network, actual nodes represent CHP, while virtual nodes represent medicinal properties (nature, flavor, and meridian tropism). Virtual nodes are connected to multiple CHP nodes with shared medicinal properties through hyperedges, forming a hierarchical hypergraph structure that supports the modeling of complex interactions.

The GTN leverages global attention mechanisms to capture long-range interactions, making it suitable for handling complex dependencies between distant nodes in formulas (Figure 4B). The HGNN aggregates medicinal property information through hyperedges, enhancing the representation of high-order structural relationships (Figure 4C). The GAT dynamically adjusts information propagation weights via edge-specific attention mechanisms, focusing on critical interactions among CHP and excelling in identifying key nodes within formulas (Figure 4D). Preliminary experiments indicated that increasing the number of network layers did not significantly improve model performance and could lead to overfitting. Consequently, GTN was designed with a single hidden layer, while HGNN and GAT used two and three hidden layers, respectively. This configuration ensured robust attention interaction among nodes, improved interpretability, and enhanced modeling efficiency and stability.

To optimize model performance, a two-stage grid search combined with five-fold cross-validation was employed to tune structural parameters (`hidden_dim`, `num_heads`, `dropout_rate`) and training parameters (`learning_rate`, `batch_size`). The optimal parameters were: GTN (`hidden_dim`=64, `num_heads`=8, `dropout_rate`=0.3, `learning_rate`=0.0007, `batch_size`=128), HGNN (`hidden_dim`=96, `num_heads`=4, `dropout_rate`=0.5, `learning_rate`=0.0005, `batch_size`=64), and GAT (`hidden_dim`=64, `num_heads`=4, `dropout_rate`=0.5, `learning_rate`=0.0001, `batch_size`=32). These optimized configurations provided a solid foundation for maximizing model performance (optimization process detailed in Figure S11 and Data S2).

Model performance was evaluated across five TCM syndrome categories—metabolic and circulatory imbalance, organ aging and immune deficiency, lifestyle and environmental factors, mental stress and external stimuli, and internal pathological changes and infections—using metrics such as AUC, precision, recall, F1 score, accuracy, and specificity (Table S1). AUC was emphasized as a key metric to assess the model's ability to distinguish unlabeled negative samples. Results showed that GTN achieved an F1 score of 0.76 on the “lifestyle and environmental factors” category but had limited performance in the “mental stress and external stimuli” category, with an AUC of only 0.62, highlighting its limitations in long-range interaction modeling (Figure 4E). HGNN demonstrated strong high-order relationship modeling in the “metabolic and circulatory imbalance” category, achieving an AUC of 0.90 on the test set (Figure 4F). However, it showed lower precision (0.16) in the “organ aging and immune deficiency” category, suggesting potential false positives. In contrast, GAT outperformed other models across all categories, achieving AUCs above 0.75, particularly excelling in the “mental stress and external stimuli” (AUC=0.76) and “organ aging and immune deficiency” (AUC=0.81) categories (Figure 4G), demonstrating its adaptability for complex relationship modeling.

To elucidate model prediction mechanisms, we analyzed the contribution of different features and nodes to AUC through feature ablation and node masking methods (data available in Data S3). Results showed that the Combination feature contributed the most to AUC, underscoring its central role in capturing herbal compatibility relationships. Sources and Medicinal properties features ranked second, while Dosage weight had the lowest contribution (Figure 4H). Node analysis revealed that CHP nodes had the highest impact on model predictions, with AUC significantly decreasing after masking. In contrast, Therapeutic nature, Medicinal flavor, and Meridian tropism nodes had comparatively lower contributions to the overall model (Figure 4I). Further analysis of feature and node masking impacts (Figure S12) reinforced the critical roles of Combination features and CHP nodes in the model.

In summary, the graph encoding method based on virtual nodes significantly enhanced the modeling of multi-dimensional relationships in CHF. The GAT model, with its superior classification performance and feature interpretability, demonstrated strong potential for unraveling complex compatibility mechanisms. The study identified CHP nodes and Combination features as core factors for CHF prediction. Additionally, the research outcomes and methods have been made publicly available (<https://github.com/ZENGJingqi/GraphAI-for-TCM>), enabling users to rapidly analyze prediction results and attention weights among CHP, thereby providing a scientific basis and data support for further exploration of CHF compatibility mechanisms.

Compatibility mechanisms in Chinese herbal formulas used for COVID-19 management

This study analyzed 215 CHF used in the prevention and treatment of COVID-19. These formulas were sourced from guidelines issued by various provincial health commissions, TCM administrations, and local governments across China. Among them, 186 formulas (Figure 5A) were derived from regional treatment guidelines, while 29 were guiding formulas listed in the *Diagnosis and Treatment Protocol for Novel Coronavirus Pneumonia* (Trial Version 8) issued by China's National Health Commission. These formulas were designed for adult patients, comprising 167 therapeutic formulas and 48 preventive formulas (details available in Data S4). Using the GAT model, the distribution of these formulas across five TCM syndrome categories showed that most were classified under the "internal pathological changes and infection factors" category (Figure 5B). This distribution aligns with TCM's understanding of COVID-19 etiology

[3], validating the model's ability to capture disease-specific mechanisms (raw prediction data provided in Data S5).

To further investigate the compatibility mechanisms, we analyzed the usage frequency of CHP and their attention weights in the model. Results (Figure 5C) showed that Licorice (CHP01118), Honeysuckle (CHP01958), and Forsythia (CHP02298) appeared most frequently in the formulas, highlighting their importance in COVID-19 management. Among these, honeysuckle and forsythia form a classic herb pair for anti-inflammatory and detoxifying effects (Figure 5D). Their high frequency and attention weights underscore their synergistic antiviral and anti-inflammatory effects, making them a key herb pair in COVID-19 formulas (frequency and weight data available in Data S6).

Radix Astragali (CHP01717) stood out prominently. Not only did it exhibit high usage frequency and significant attention weight, but it also played a central role in multiple herb pairs, such as Radix Astragali-Perilla (CHP01717-CHP05676) and Radix Astragali-Coix Seed (CHP01717-CHP00216). This indicates that Radix Astragali likely functions as the “sovereign herb” in COVID-19 formulas, primarily responsible for immune modulation and core efficacy, while other herbs like perilla and coix seed serve as “minister” or “assistant” herbs to enhance or coordinate its effects. For instance, in the Huashi Baidu Decoction [17], attention analysis showed that Radix Astragali (CHP01717) had significantly higher attention weights toward other CHP compared to other herbs (Figure 5E), further confirming its central role in compatibility.

KEGG pathway enrichment analysis of Radix Astragali's compound-target interactions revealed that its primary mechanisms involve the neuroactive ligand-receptor interaction pathway [18], the MAPK signaling pathway [19], and the calcium signaling pathway [20] (Figure 5F). These pathways are closely associated with inflammation regulation, immune modulation, and antiviral effects, further highlighting its significance in COVID-19 management.

Compound analysis showed that the pharmacological effects of Radix Astragali are primarily driven by three classes of chemical constituents: terpenoids, alkaloids, and shikimates and phenylpropanoids (Figure 5G). By filtering compound-target pairs with binding affinities >8.0 , a component- compound-target-KEGG pathway network for Radix Astragali was constructed (Figure 5H). This network demonstrated that high-binding-affinity compounds are broadly involved in the aforementioned key pathways, further confirming their pharmacological importance (network data available in Data S7).

Combining compound drug-likeness screening, Figure 5I identified potential active molecules in Radix Astragali with high drug development potential. These molecules, characterized by strong binding abilities and extensive target coverage, are promising candidates for drug discovery.

In conclusion, this study utilized a graph neural network model to analyze attention weights among CHP and identified Radix Astragali as a core herb in COVID-19 formulas. The findings elucidated its key role in compatibility mechanisms and provided a scientific basis and data support for related pharmacological research and drug development.

Discussion

This study applied GraphAI technologies combined with TCM theories to quantitatively analyze the complex compatibility mechanisms in CHF. It addresses longstanding challenges in TCM research, such as the difficulty of quantifying herbal synergy, the lack of model interpretability, and the scarcity of high-quality data resources. By employing the GAT model, we uncovered the synergistic effects among herbs, quantified the contributions of core CHP, and opened new avenues for modern TCM research and drug discovery.

Unlike other studies focusing on formula recommendations [21-24], our research centers on elucidating the compatibility mechanisms of clinically validated formulas rather than designing new ones from scratch. Our model integrates TCM theoretical foundations through the introduction of virtual medicinal property nodes and multi-dimensional feature representations, offering a high level of interpretability. The feature outputs generated by GAT models can be transferred to small-sample problems in specific diseases, breaking the "black-box" limitations of deep learning models. This approach provides a novel method for modeling and understanding the complex systems of TCM, supporting the optimization and generation of existing formulas while laying a foundation for material basis research and new drug development.

The "sovereign-minister-assistant-courier" framework is central to TCM compatibility theory. For the first time, we proposed a quantitative method using GraphAI to evaluate the contribution of CHP in formulas via attention mechanisms. Results revealed that core herbs such as Radix Astragali dominate in several high-frequency herb pairs. KEGG pathway enrichment analysis confirmed its immunomodulatory role. Radix Astragali's pivotal function in regulating inflammation and immune responses highlights its role as the "sovereign herb" in COVID-19 treatment formulas, providing clear directions for further formula optimization and material basis exploration.

Long COVID is a complex post-infection syndrome involving immune dysregulation, viral persistence, and endothelial dysfunction [25]. Our findings suggest that Radix Astragali, through mechanisms such as the MAPK signaling pathway, calcium signaling pathway, and neuroactive ligand-receptor interaction, exhibits significant immunomodulatory and anti-inflammatory effects. This indicates that formulas centered on Radix Astragali may offer effective strategies for managing long COVID. For example, a preventive formula proposed in Shanghai for general populations (Radix Astragali 15g, Reed Rhizome 15g, Lotus Leaf 6g, Patchouli 6g, Perilla Leaf 6g, and Mint 3g) warrants attention. Composed entirely of food-medicinal herbs with high safety, this formula is suitable for general use and has potential for improving immune function and balancing metabolic states, making it a viable option for long COVID patients.

While compound-target analysis is an important approach to understanding drug mechanisms, the efficacy of TCM is not limited to the actions of small-molecule compounds [1]. This study emphasized the holistic synergistic effects of herbal combinations alongside compound-target mechanisms. The interactions among CHP may produce more significant pharmacological effects through multi-target synergy. This dual focus on holistic efficacy and mechanistic components offers a new paradigm for comprehensively understanding TCM.

A key highlight of this study is the open availability of data and code (<https://zenodo.org/records/13763953> and <https://github.com/ZENGJingqi/GraphAI-for-TCM>),

providing high-quality resources for academic research and fostering interdisciplinary collaboration and technological innovation. Our technical framework is adaptable to other traditional medical systems, such as Uyghur medicine, allowing exploration of unique medicinal theories and disease management strategies from diverse cultural contexts. This approach not only helps elucidate the commonalities and differences among various medical systems but also offers new perspectives for global healthcare services.

In conclusion, this study proposed an innovative method for quantifying TCM compatibility mechanisms and validated the modernized potential of TCM theories by elucidating Radix Astragali's core role in COVID-19 treatment formulas. Looking forward, we aim to expand this framework, develop multi-expert systems, and advance the scientific foundation of TCM theories and practices. This effort will optimize healthcare services and drug development processes, contributing to the modernization of traditional medicine worldwide.

Acknowledgements

This work benefited from the integration of data from numerous open-access and authoritative databases. We acknowledge the valuable contributions of resources such as DrugBank, BindingDB, BioGRID, DisGeNET, the *World Health Organization International Standard Terminologies on Traditional Chinese Medicine*, and many others. These datasets provided essential insights into Traditional Chinese Medicine, modern drug chemistry, genetics, diseases, and related fields, forming the foundation for the TCM Multi-dimensional Knowledge Graph (TCM-MKG) used in this study. Furthermore, we utilized the PSICHIC model (<https://github.com/huankoh/PSICHIC>) to analyze the binding interactions between components and targets. Full citations for these resources are included in the manuscript.

Funding

This research was supported by the National Natural Science Foundation of China (Grant No. 82230117, Xiaobin Jia). The funders of the study had no role in study design, data collection, data analysis, data interpretation, or writing of the report.

Authors' contributions

Conceptualization: Xiaobin Jia ; Methodology: Jingqi Zeng; Investigation: Jingqi Zeng; Data curation: Jingqi Zeng; Formal analysis: Jingqi Zeng; Software: Jingqi Zeng; Validation: Jingqi Zeng; Visualization: Jingqi Zeng; Funding acquisition: Xiaobin Jia; Project administration: Xiaobin Jia; Supervision: Xiaobin Jia; Writing – original draft: Jingqi Zeng; Writing – review & editing: Jingqi Zeng, Xiaobin Jia.

Competing interests

The authors declare that they have no competing interests.

Data and materials availability

All data and code used in this study are openly available. The TCM multi-dimensional knowledge graph (TCM-MKG) is accessible at <https://zenodo.org/records/13763953>, and the graph artificial intelligence model implementation is available at <https://github.com/ZENGJingqi/GraphAI-for-TCM>.



Fig. 1. Data structure and component-target analysis in the TCM-MKG. (A) Overview of the TCM-MKG database structure, including TCM terminology, Chinese patent medicines (CPM), Chinese herbal pieces (CHP), natural products (NP), chemical components, targets, and diseases. (B) Distribution of the number of Chinese herbal pieces per CPM. (C) Dosage ratio distribution of Chinese herbal pieces in CPMs. (D) Presence of compound targets in the TCM database. (E) UMAP visualization of molecular descriptors, Morgan fingerprints, and graph-based models: graph convolutional network (GCN), graph attention network (GAT), and graph autoencoder (GAE). (F) Binding affinity distribution of three datasets: diffused TCM targets (7,260,578 samples), high-fidelity targets (283,793 samples), and recorded TCM targets (343,373 samples), with a random control of 10,000 non-TCM targets. (G) Number of EntrezIDs per InChIKey across binding affinity thresholds. (H) InChIKey coverage across binding affinity thresholds. (I) EntrezID coverage across binding affinity thresholds.

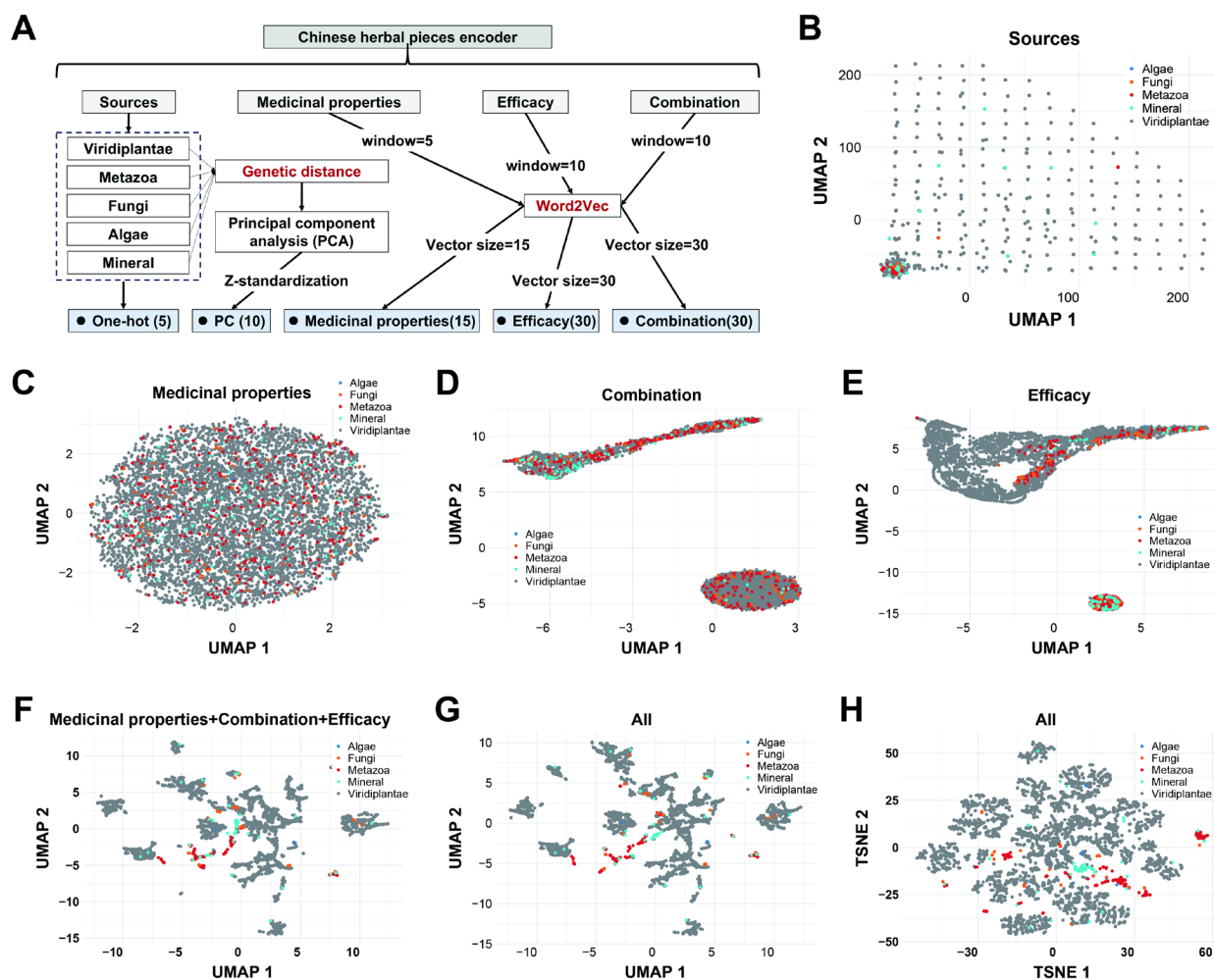


Fig. 2. Multi-feature encoding and dimensionality reduction analysis of Chinese herbal pieces. (A) Workflow of multi-feature encoding for Chinese herbal pieces. Features include sources (encoded with one-hot and principal component analysis, PCA), medicinal properties (vectorized using Word2Vec with window size = 5 and vector size = 15), efficacy (vectorized using Word2Vec with window size = 10 and vector size = 30), and combination relationships (vectorized using Word2Vec with window size = 10 and vector size = 30). Z-standardization was applied where necessary. Encoded feature dimensions are labeled as: sources one-hot (5), sources PCA (10), medicinal properties (15), efficacy (30), and combination (30). (B) UMAP projection of source features. (C–E) UMAP projections of features representing medicinal properties, combination relationships, and efficacy, respectively. (F) UMAP projection of combined features: medicinal properties, combination, and efficacy. (G) UMAP projection of all combined features, integrating sources, medicinal properties, efficacy, and combination. (H) t-SNE projection of all combined features.

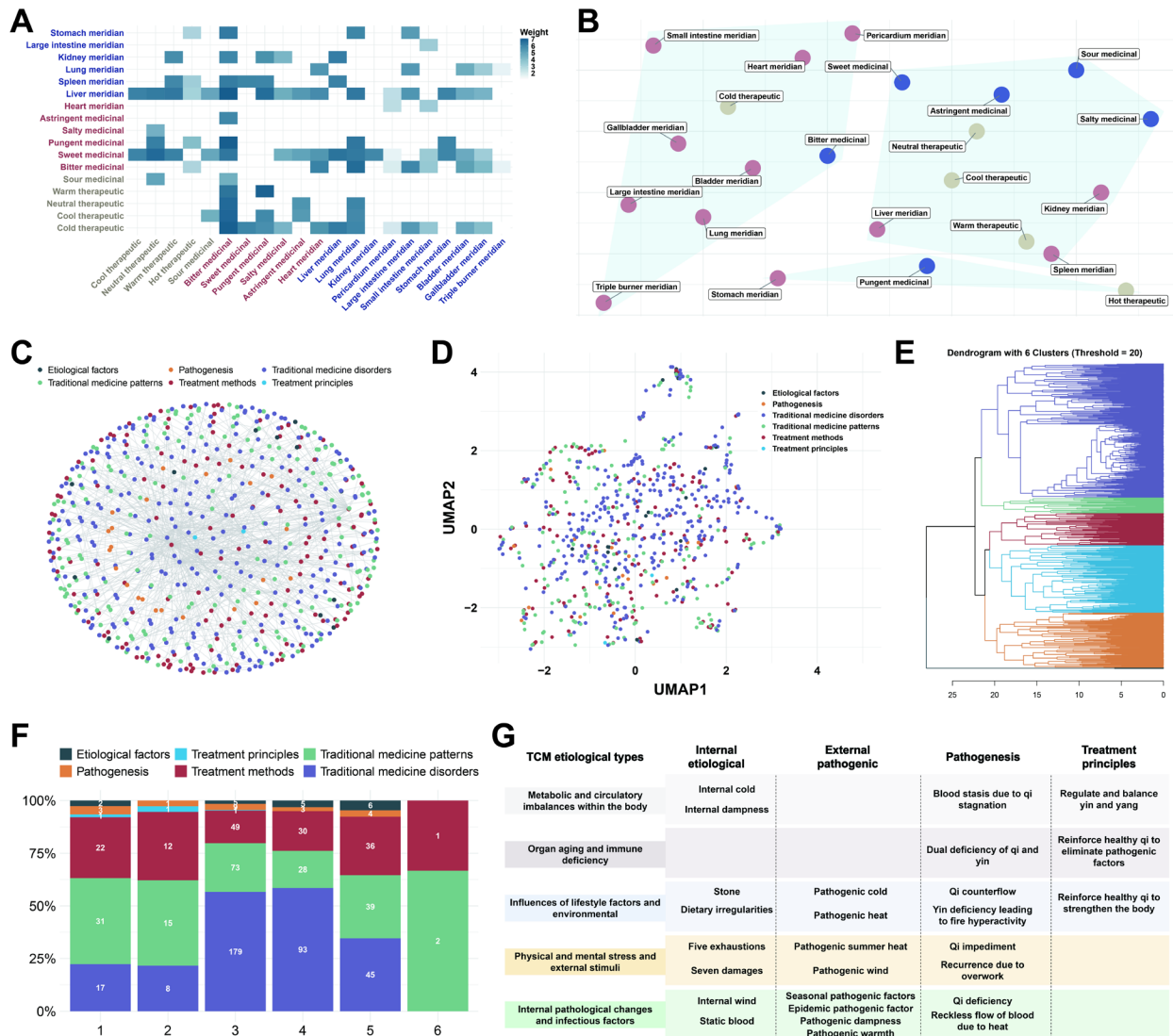


Fig. 3. Analysis of medicinal properties and TCM diagnostic terminology. (A) Heatmap showing the association strengths between medicinal properties of Chinese herbal pieces, categorized into therapeutic nature, medicinal flavor, and meridian tropism. (B) Network distribution of medicinal properties, visualized with community detection and optimized layout, highlighting functional modules and interrelationships. (C) Network structure of TCM diagnostic terminologies, encompassing etiological factors, pathogenesis, traditional medicine patterns, treatment methods, and treatment principles, encoded into 32-dimensional vectors using Node2Vec. (D) UMAP projection of TCM diagnostic terminologies. (E) Hierarchical clustering dendrogram of TCM diagnostic terminologies, classified into six major groups. (F) Proportional distribution of diagnostic terminologies across six TCM etiological categories. (G) Diagnostic characteristics of five major TCM etiological types, detailing internal etiological factors, external pathogenic factors, pathogenesis, and treatment principles. The sixth category is excluded due to insufficient data.

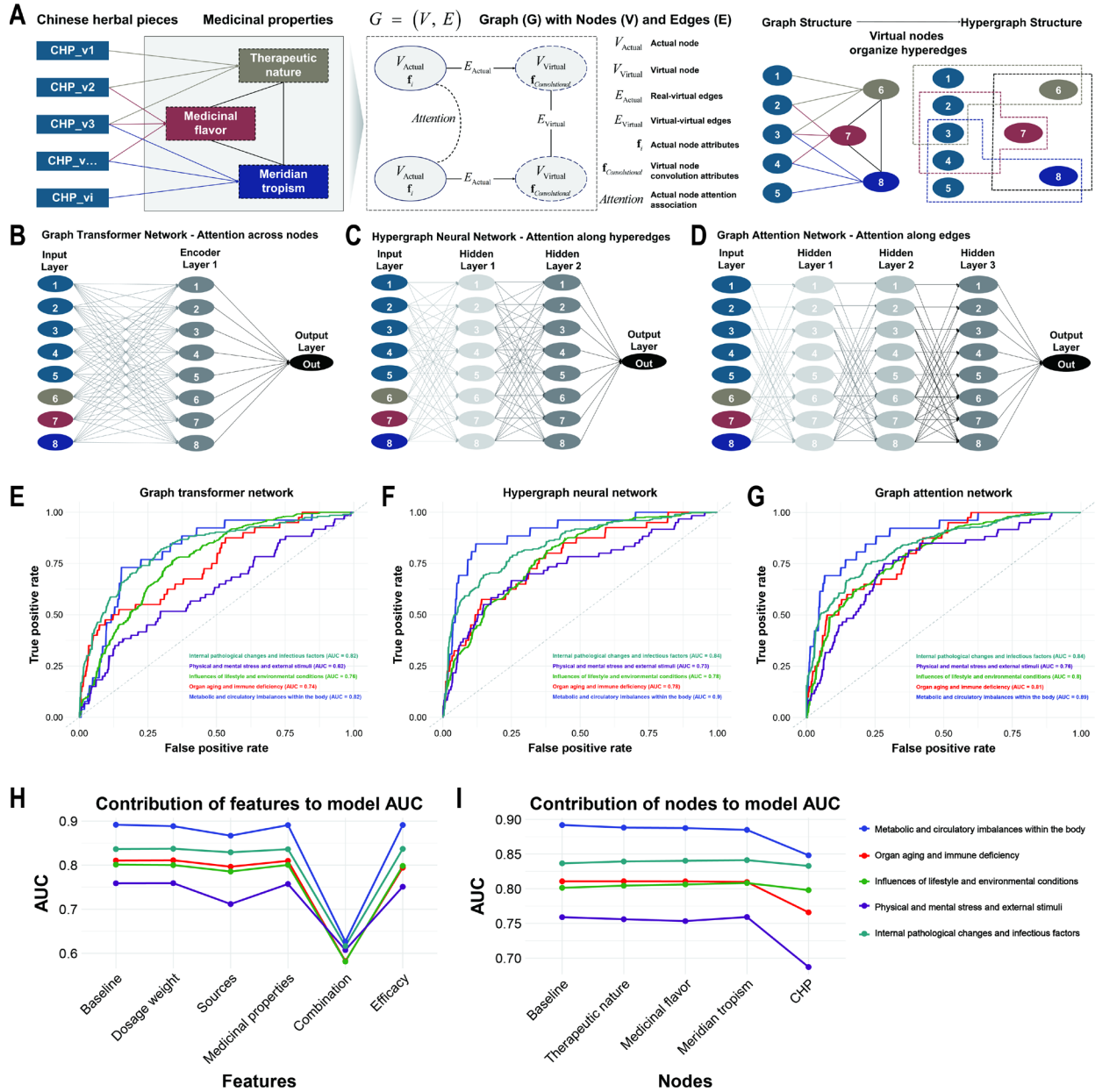


Fig. 4. Graph encoding and attention mechanisms for Chinese herbal formulas. (A) Graph structure encoding the relationships between Chinese herbal pieces and their medicinal properties, represented by virtual nodes for therapeutic nature, medicinal flavor, and meridian tropism. Virtual nodes enable transformation into hypergraph structures for advanced modeling. (B–D) Architectures of graph models: (B) graph transformer network, (C) hypergraph neural network, and (D) graph attention network. (E–G) AUC performance curves for (E) graph transformer network, (F) hypergraph neural network, and (G) graph attention network, across five major TCM etiological categories. (H–I) Contributions to model AUC evaluated using the zeroing method: (H) feature-level contributions and (I) node-level contributions, both based on the graph attention network.

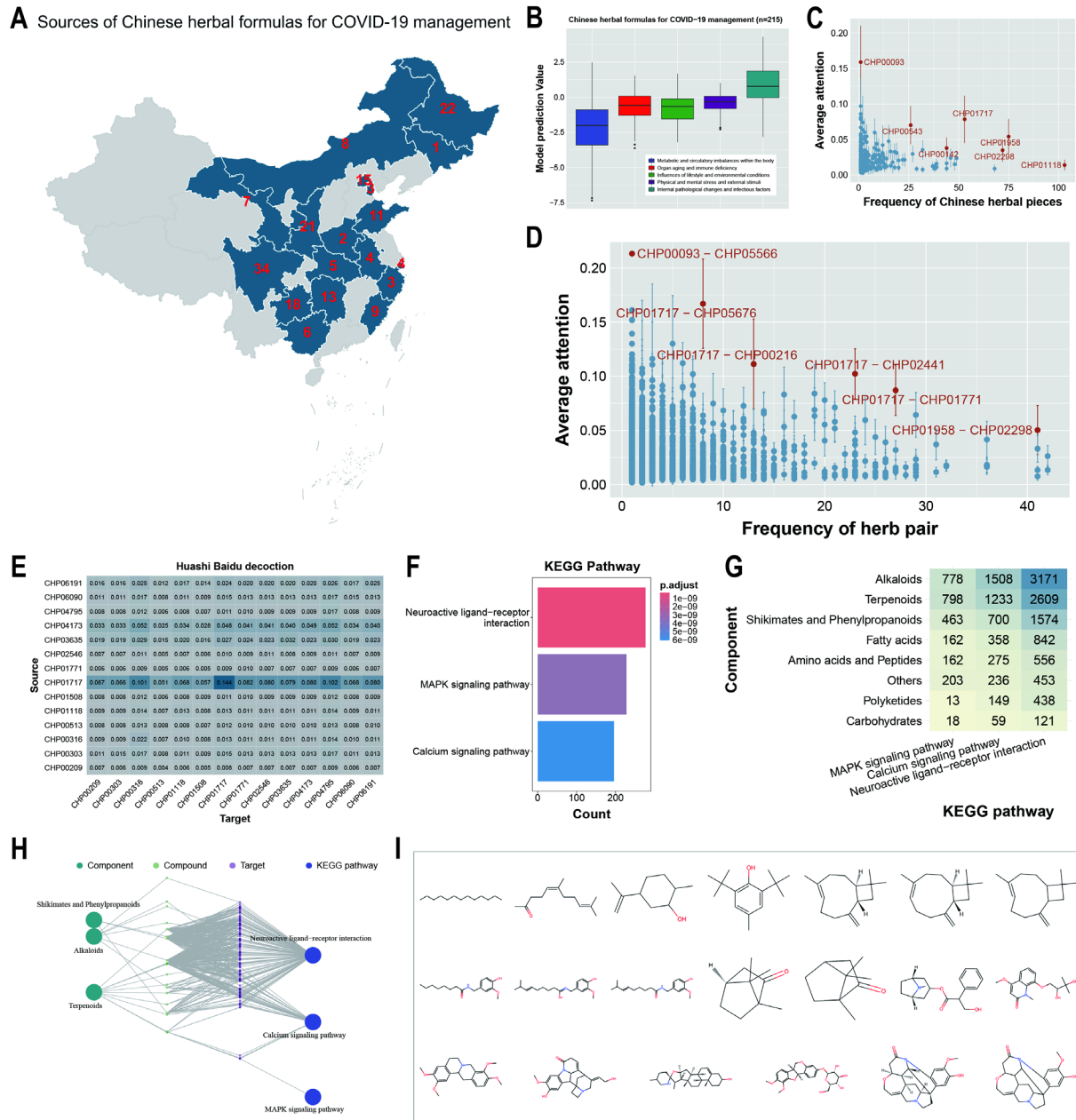


Fig. 5. Analysis of compatibility mechanisms in Chinese herbal formulas for COVID-19 management. (A) Geographic distribution of 215 Chinese herbal formulas across China, excluding 29 nationwide formulas from the National Health Commission. (B) Model-predicted outcomes of the formulas across five major TCM etiological categories. (C–D) Frequency and average attention weights of Chinese herbal pieces and herb pairs in the formulas, with key elements highlighted based on high frequency or significant attention weights. (E) Attention weights of Chinese herbal pieces in the Huashi Baidu Decoction, with darker heatmap colors indicating higher weights and numerical values displayed. (F) Top three KEGG pathways enriched for Radix Astragali (CHP01717) targets. (G) Contributions of Radix Astragali component to KEGG pathways, with numbers indicating compound-target pairs per pathway. (H) Component-compound-target-KEGG pathway network for Radix Astragali. (I) Key bioactive compounds of Radix Astragali with predicted binding affinities >8.0 to targets in enriched KEGG pathways.

Supplementary Materials

The PDF file includes:

Materials and Methods

Supplementary Text

Figs. S1 to S12

Tables S1

References (26–51)

Data S1 to S7

Materials and Methods

TCM terminology module

The TCM terminology module forms the semantic foundation of the TCM-MKG. Systematic categorization and standardization ensure semantic consistency across modules. This module is based on the *WHO International Standard Terminologies on Traditional Medicine* (2022 edition), comprising 1,810 core TCM terms (ISBN: 9789240042322), including key concepts like etiology, pathogenesis, therapeutic principles, and treatments. These terminologies provide theoretical support for cross-module data interconnectivity. The standard, published by the World Health Organization (WHO), is accessible at: <https://www.who.int/publications/i/item/9789240042322>.

Chinese patent medicine module

The CPM module integrates data on 8,977 Chinese patent medicines, including formula composition, dosage forms, efficacy, indications, and their links to modern medical diseases. The primary data sources include the *Chinese Pharmacopoeia* (2020 edition) and the *China Medicine Information Query Platform* (www.dayi.org.cn). Moreover, the indications of CPM formulas are mapped to ICD-11 codes using the ICD-11 coding tool (<https://icd11.pumch.cn>) to bridge traditional Chinese and modern Western medical systems.

Chinese herbal pieces module

The CHP module documents 6,207 Chinese herbal pieces, encompassing fundamental information such as medicinal properties, biological sources, and chemical compositions. This module supports systematic investigations into the mechanisms of action and chemical characteristics of CHP. Key data sources include the *Chinese Pharmacopoeia* (2020 edition), the *China Medicine Information Query Platform* (www.dayi.org.cn), and NCBI Taxonomy (<https://www.ncbi.nlm.nih.gov/taxonomy>) [26], which converts Latin species names into standard identifiers. Chemical composition data were integrated from authoritative databases and lab-cultured sources, including: TCMID V2.0 (<http://47.100.169.139/tcmid>) [27], TCMbank V1.0 (<https://tcmbank.cn>) [28], SymMap V2.0 (<http://www.symmap.org>) [29], HIT V2.0 (<http://hit2.badd-cao.net>) [30], HERB V2.0 (<http://47.92.70.12>) [31], ETCM V2.0 (<http://www.tcmip.cn/ETCM2>) [32] and TCMSP V1.0 (<https://www.tcmisp-e.com/>) [33].

Natural products module

The NP module records 4,810 natural products, detailing their biological sources, chemical compositions, and related information. This module provides a systematic basis for studying natural products in TCM, supporting research from pharmacological effects to molecular mechanisms. Data primarily originate from NCBI Taxonomy (<https://www.ncbi.nlm.nih.gov/taxonomy>) [26], ensuring accurate classification of natural products (e.g., family, genus, species). Shared chemical composition data link the NP and CHP modules. Additional data were sourced from the **CMAUP database** (<https://www.bidd.group/CMAUP/index.html>) [34]. For natural products identified as CHP, mapping is achieved through CHP-NP associations. For those recorded directly as natural products (e.g., plants or fungi identified by Latin names), chemical composition data were directly compiled.

Chemical compounds module

The chemical compounds module systematically documents information on 123,647 chemical compounds, including basic structural data, target associations, and cross-database mappings. This module provides a robust data foundation for elucidating the molecular mechanisms of TCM and pharmacological research. All chemical compounds were standardized using RDKit (<https://www.rdkit.org/>), with InChIKey as the unique identifier to ensure consistency and traceability. Fundamental data include SMILES, InChI, and Molecular_formula, while molecular descriptors generated by RDKit (e.g., molecular weight, logP, and topological polar surface area) support structural analysis and efficacy evaluations.

To classify chemical structures systematically, NPClassifier V1.5 (<https://npclassifier.ucsd.edu/>) [35] was used for three-tier classification (Pathway, Superclass, and Class) and for annotating IsGlycoside information to identify glycoside compounds. This classification reveals the biological characteristics and pharmacological activities of the compounds. Chemical compound-target association data were integrated from the following sources: DrugBank V5.1.12 (<https://go.drugbank.com>) [36]; TTD (<https://db.idrblab.net/ttd/>) [37]; STITCH V5.0 (<http://stitch.embl.de>) [38]; BindingDB (<https://www.bindingdb.org>) [39]. All targets were human-specific and identified using EntrezID for standardization. Beyond chemical compounds derived from CHP and natural products, the module includes all compounds from DrugBank and TTD, as well as compound-target associations from STITCH with a confidence score exceeding 700, providing high-quality training data for target prediction.

Targets module

The targets module in the TCM-MKG contains 20,053 standardized human targets and their detailed features, along with 6,879,008 protein-protein interaction (PPI) records. This module systematically supports TCM target research and network biology analyses. Target data were standardized using multiple identifiers, including EntrezID, UniProtID, GeneSymbol, and ENSGID, ensuring compatibility and traceability. Target symbols and sequence information were derived from Ensembl GRCh37.p13 (http://grch37.ensembl.org/Homo_sapiens/Info/Index) [40] and UniProt Release 2024_02 (<https://www.uniprot.org/>) [41]. Each target entry includes multiple standard identifiers and protein sequence data. Protein-protein interaction data were integrated from the following resources: STRING V12.0 (<https://cn.string-db.org/>) [42]; SIGNOR V3.0 (<https://signor.uniroma2.it/>) [43]; MINT (<https://mint.bio.uniroma2.it/>) [44]; IntAct (<https://www.ebi.ac.uk/intact/home>) [45]; BioGRID V4.4.233 (<https://thebiogrid.org/>) [46]. These

databases provide extensive information on direct protein-protein interactions and causal relationships.

Disease module

The disease module in the TCM-MKG integrates core data from the 2024 Chinese and English versions of ICD-11 and extends this data through standardized mappings to multiple authoritative databases, including the NCBI Unified Medical Language System (UMLS, <https://uts.nlm.nih.gov/uts/umls>), Medical Subject Headings (MeSH, <https://uts.nlm.nih.gov/uts/umls>) [47], and the Disease Ontology (DOID, <https://disease-ontology.org/do>) [48]. This module includes multi-layered mappings between ICD-11 codes and corresponding UMLS Concept Unique Identifiers (CUIs), MeSH identifiers, and DOIDs, covering 12 semantic types such as diseases or syndromes, neoplastic processes, signs or symptoms, and injuries or poisoning. It comprises 65,758 CUI mapping records, 6,853 MeSH mapping records, and 4,803 DOID mapping records. These multi-dimensional mappings enable standardized disease data management and cross-platform queries.

Disease-target association data were integrated from multiple authoritative databases. CUI-classified disease-target associations were sourced from DisGeNET V7.0 (<https://www.disgenet.org/>) [49], totaling 575,153 records. MeSH-classified disease-target associations were obtained from the Comparative Toxicogenomics Database (CTD, <https://ctdbase.org/>) [50], comprising 24,097,586 records. DOID-classified disease-target associations were derived from Diseases V2.0 (<https://diseases.jensenlab.org/>) [51], totaling 6,522,131 records.

Encoding medicinal properties of Chinese herbal pieces and network construction

This study systematically encoded and analyzed the medicinal properties of CHP using standardized processing and graph intelligence methods. The medicinal properties included therapeutic nature, medicinal flavor, and meridian tropism, which were organized into a hierarchical classification to build a medicinal property knowledge graph. To quantify the relationships among these attributes, we constructed an undirected network model, where nature, flavor, and meridian tropism were represented as nodes, and the edge weights reflected the strength of their associations.

The initial network layout was based on the logical framework of medicinal property theory, subsequently optimized using the ForceAtlas2 algorithm for enhanced visual clarity. Key parameters included an edge weight influence of 1.0, jitter tolerance of 0.1, Barnes-Hut optimization setting of 1.2, and the activation of a strong gravity mode (gravity value: 5.0). To identify potential functional modules within the network, the Louvain method was applied for community detection, grouping nodes into distinct communities based on edge weights, with modular distribution visually represented through color coding.

Encoding and clustering of TCM diagnostic terms

To analyze the multi-dimensional relationships among TCM diagnostic terms, we applied the Node2Vec algorithm, embedding diagnostic features such as etiology, pathogenesis, treatment principles, and therapeutic methods into a 32-dimensional vector space. A graph model was

constructed with formulas and their diagnostic features as nodes, and their relationships were represented as edge weights. The high-dimensional feature embeddings were reduced to a two-dimensional space using UMAP to reveal potential relationships among diagnostic terms.

Hierarchical clustering was subsequently performed on the 32-dimensional feature vectors to classify the diagnostic terms into six categories, with the proportion of etiology, pathogenesis, treatment principles, and therapeutic methods calculated for each category. Due to the small sample size of category six, analysis focused on the primary five categories. Core features for each category were extracted using centroid vectors to support naming.

Graph encoding of Chinese herbal formulas and message passing mechanisms

To quantify the complex relationships between CHP and medicinal properties within CHF, we designed a graph encoding method using virtual nodes. This method integrates core concepts of TCM theory with modern GNN techniques for a hierarchical and quantitative analysis of formula compatibility. The graph structure consisted of real nodes and virtual nodes. Real nodes represented CHP, with attributes including 91 feature variables (90 describing characteristics such as efficacy and origin, and one for dosage, set to zero if unknown). Virtual nodes represented medicinal property categories, including "Therapeutic nature," "Medicinal flavor," and "Meridian tropism," with initial attributes calculated as the weighted mean of all connected real node attributes. Edge attributes quantified the relationships between CHP and medicinal properties using a two-dimensional encoding.

To represent the complex relationships more comprehensively within formulas, virtual node attributes dynamically updated based on the attributes of connected real nodes, calculated as the weighted mean of all linked node attributes. Edge attributes between virtual nodes were determined by averaging the attributes of all connected real-node edges, reflecting potential relationships among medicinal property categories. This design, through virtual nodes connecting multiple real nodes, established a hierarchical hypergraph structure for CHF, facilitating the discovery of complementary and interactive relationships among CHP.

After constructing the graph structure, we implemented three GNN models to capture the multi-dimensional relationships within CHF: Graph Transformer Network (GTN): Captures long-range interactions using a global attention mechanism between nodes. A single-layer hidden design balances complexity and computational efficiency. Hypergraph Neural Network (HGNN): Leverages hyperedges to organize high-order structural relationships between virtual and real nodes, using two hidden layers to enhance information aggregation. Graph Attention Network (GAT): Dynamically adjusts message-passing weights through edge attention mechanisms, focusing on key interactions among CHP. A three-layer hidden structure captures multi-level node interactions. This design ensures that every node in the model interacts attentively with others, achieving high interpretability while improving modeling efficiency and stability.

Data selection and grouping for graph neural network models

This study utilized a dataset containing 6,080 CHF, categorized into five major disease types: metabolic and circulatory imbalance, organ aging and immune deficiency, lifestyle and environmental impacts, psychological stress and external stimuli, and internal pathological changes with infectious factors. The dataset was split into training (4,256 samples), validation

(1,222 samples), and test (602 samples) sets in a 7:2:1 ratio. The positive sample proportions for the five disease types in the training, validation, and test sets were as follows: metabolic and circulatory imbalance (6.34%, 6.87%, 4.32%), organ aging and immune deficiency (6.41%, 6.79%, 6.64%), lifestyle and environmental impacts (57.31%, 57.77%, 57.81%), psychological stress and external stimuli (10.10%, 9.17%, 9.97%), and internal pathological changes with infectious factors (30.45%, 30.03%, 32.56%). To comprehensively evaluate model performance across the five disease types, multiple metrics were employed, including precision, recall, F1 score, area under the curve (AUC), accuracy, and specificity.

Hyperparameter optimization

To optimize the performance of the three GNN models—GTN, HGNN, and GAT—a two-stage grid search strategy was employed, combined with 5-fold cross-validation using the full dataset of 6,080 samples. In the first stage, model structural parameters were tuned, including hidden layer dimensions (hidden_dim: 32, 64, 96, 128), number of attention heads (num_heads: 2, 4, 8, 16), and dropout rates (dropout_rate: 0.1, 0.3, 0.4, 0.5). The average loss on the validation set was used to assess the performance of each parameter combination, and the configuration with the lowest loss was selected as the optimal structural parameter set. In the second stage, training parameters such as learning rate (learning_rate: 0.0001, 0.0003, 0.0005, 0.0007) and batch size (batch_size: 16, 32, 64, 128) were optimized. These combinations were evaluated based on the average loss on the validation set, with the lowest loss configuration chosen as the optimal training setup. To ensure stability, all parameter searches employed 5-fold cross-validation, using the mean validation loss as the evaluation metric. Detailed results of the optimization process and raw data are available in the supporting materials (Figure S11 and Data S2).

Model interpretability analysis

To assess the contribution of features and nodes in the models, this study employed the feature nullification method for interpretability analysis of the GAT model. The feature nullification method involves setting specific feature values to zero (nullification) and observing changes in model performance (AUC), thereby quantifying the importance of each feature to prediction outcomes. For node contribution analysis, all features of specific nodes (e.g., dosage, medicinal properties) were nullified one at a time, and the AUC before and after nullification was compared to evaluate the node's impact on prediction results. All analyses were conducted on the test set to avoid overfitting and ensure the representativeness and robustness of interpretability results. Raw data from these analyses are available in Data S3.

Supplementary Text

Impact of feature representation methods and neighbor distances on predicted binding affinity

In predicting binding affinity for TCM compound-target interactions, both feature representation methods and neighbor distances exhibited clear trends. Overall, shorter neighbor distances corresponded to higher predicted binding affinities, a pattern consistent across all feature representation methods. This finding underscores that compounds with similar features are more likely to bind to high-affinity targets.

Specifically, traditional feature representations such as molecular descriptors (Figure S1A) and molecular fingerprints (Figure S1B) showed that compounds with shorter neighbor distances were

primarily distributed in the moderate binding affinity range (5.0–7.5). This suggests that traditional molecular features effectively capture local structural similarities, enabling accurate predictions in the mid-affinity range. However, their performance in the high-affinity range (8.0–10.0) was weaker, indicating limitations in representing complex molecular features.

Feature representations derived from graph neural networks demonstrated significant advantages in binding affinity prediction. The Graph Autoencoder (GAE, Figure S1C) and Graph Convolutional Network (GCN, Figure S1E) not only performed well in the moderate affinity range (5.0–7.5) but also showed a notable presence in the high-affinity range (8.0–10.0). This highlights the ability of GAE and GCN to extract deeper features from molecular graph structures, capturing both local similarities and molecular properties associated with high-affinity targets. At shorter neighbor distances, these methods showed a high concentration of predictions in the high-affinity range. As neighbor distances increased, the high-affinity distribution gradually diminished, indicating their strength in identifying high-quality similarities within short distances.

The Graph Attention Network (GAT, Figure S1D) exhibited intermediate performance between traditional molecular features and GAE/GCN. While GAT also showed high binding affinity predictions at shorter neighbor distances, its distribution was primarily concentrated in the moderate affinity range (5.0–7.5). Its ability to identify high-affinity targets was relatively limited. This suggests that although GAT's multi-head attention mechanism optimizes the representation of compound-target similarities, it is less effective than GAE and GCN in capturing complex features associated with high-affinity targets.

To further quantify the performance of each method in binding affinity prediction, we calculated the average binding affinity within short neighbor distances (Figure S1F). Results indicated that GAE and GCN achieved significantly higher average binding affinities compared to molecular descriptors, molecular fingerprints, and GAT, confirming the superiority of these two graph neural network embeddings in predicting high-affinity targets.

Influence of molecular weight and target sequence length on binding affinity prediction

To investigate the patterns of binding affinity between TCM compounds and targets, this study analyzed “High fidelity targets”, “Recorded TCM targets”, and “TCM diffused targets” from the perspectives of molecular weight and target sequence length. These datasets revealed significant differences in binding affinity distribution, reflecting the influence of data generation methods and target selection strategies on the results.

The “High fidelity targets” dataset (Figure S2A) exhibited a concentration of high binding affinities (mean affinity > 7.5) in the region of molecular weights between 350 and 1100 Da and target sequence lengths under 1000. This distribution reflects a target-driven screening process, such as rational design or target-specific screening, where compound-target pairs with high binding affinities are selected by optimizing the compatibility of specific targets and compounds. The binding affinities in this dataset show a pronounced focus, particularly in the region combining moderate molecular weights with short sequence targets.

In contrast, the “Recorded TCM targets” dataset (Figure S2B) displayed a more dispersed distribution of binding affinities. High-affinity regions (mean affinity > 6.5) were concentrated around compounds with molecular weights of 354–454 Da, interacting with targets of varying

lengths. This distribution likely stems from compound-driven virtual screening or structure similarity-based methods for extending target associations. While this approach increases coverage, it also elevates the risk of false positives, particularly when compound-target compatibility is lower. The complex chemical structures and multi-target effects of TCM compounds further contribute to the dispersion of binding affinities.

The “TCM diffused targets” dataset (Figure S2C) showed a binding affinity distribution trend similar to “High fidelity targets.” High values (mean affinity > 7.0) were also concentrated in the region of molecular weights between 350 and 1100 Da and target sequence lengths under 1000. This indicates that the neighbor-diffusion strategy effectively inherited the characteristics of “High fidelity targets” when expanding compound-target associations. By leveraging structural similarity among compounds, the neighbor-diffusion method inferred nearby compound-target associations, ensuring that the binding affinity distribution of the candidate pairs aligns closely with that of “High fidelity targets.” This approach expands the data scope while maintaining the reliability of the predictions.

In summary, the binding affinity distribution of “High fidelity targets” is concentrated, reflecting the characteristics of target-driven design. The “Recorded TCM targets” demonstrate higher dispersion due to compound-centric expansion methods. The “TCM diffused targets” exhibit a concentrated binding affinity distribution comparable to “High fidelity targets,” proving the reliability of the neighbor-diffusion method in compound-target prediction. These findings indicate that the neighbor-diffusion method effectively expands TCM compound-target data while preserving the high confidence of predictions, providing robust data support for studying the molecular mechanisms of TCM.

Feature encoding of origin attributes for Chinese herbal pieces

Origin attributes are key features of CHP, reflecting their biological sources and evolutionary relationships. This study employed phylogenetic tree analysis and PCA to construct a 15-dimensional feature vector that comprehensively integrates biological classification and evolutionary information. The workflow and results of origin feature encoding are presented in Figure S3.

As shown in Figure S3A, the origins of CHP are predominantly from the Viridiplantae, followed by the Metazoa, minerals, Fungi, and Algae, illustrating the proportional contributions of various biological sources in TCM materials. To construct the phylogenetic tree, TaxID information of the species associated with CHP was retrieved from the NCBI Taxonomy database. Based on their taxonomic positions, a corresponding phylogenetic structure was generated. Figures S3B–F display the phylogenetic tree structures for minerals, plants, animals, fungi, and algae, respectively. Mineral drugs (Figure S3B), being non-living entities, were encoded as independent nodes, whereas other biological groups exhibit complex branching evolutionary relationships.

To quantify the origin features of CHP, PCA was performed on the phylogenetic tree distance matrix derived from species data. Figure S3G shows the cumulative explained variance of the top 10 principal components for each origin category. These top 10 components captured over 80% of the variance in origin attributes, making them suitable for feature encoding of plants, animals, and fungi. However, due to the limited sample size of algae (only seven species), a maximum of seven

principal components could be extracted. To maintain a consistent 15-dimensional feature vector, algae were encoded similarly to minerals as independent nodes, with the remaining three features supplemented by dummy variables. This approach not only preserves the unique properties of algae but also ensures the completeness of the classification.

Furthermore, the five primary origin categories (plant kingdom, animal kingdom, fungal kingdom, algal kingdom, and mineral sources) were quantitatively encoded using binary dummy variables, forming five binary features that explicitly differentiate CHP from various biological domains. These dummy variable features provide additional categorical information on origin attributes, enhancing the model's adaptability to diverse CHP sources.

In conclusion, the origin feature encoding resulted in a 15-dimensional feature vector composed of 10 principal component variables and 5 dummy variables. This encoding accurately captures the biological classification and evolutionary relationships of CHP while providing essential biological foundations for systematic CHP research.

Identification of core nodes in the Tcm diagnostic-therapeutic terminology network

To identify key nodes within the TCM diagnostic-therapeutic terminology network, this study quantitatively evaluated node importance using ten centrality metrics. These metrics included degree centrality, betweenness centrality, closeness centrality, eigenvector centrality, PageRank, harmonic centrality, clustering coefficient, average neighbor degree, k-core, and load centrality. Together, these metrics provided a comprehensive quantitative basis for assessing the status and influence of nodes in the network. Dimensionality reduction of centrality data using UMAP (Figure S10A) revealed that network nodes could be classified into three distinct categories. Network layout analysis (Figure S10B) further illustrated the spatial distribution characteristics of these categories: Category 2 nodes were located in the network's core region, Category 1 nodes occupied intermediate layers, and Category 3 nodes were predominantly found at the network's periphery.

A statistical analysis of diagnostic-therapeutic terminology distribution across the node categories (Figure S10C) revealed that Category 2 nodes were primarily associated with therapeutic principles and methods, forming the core components of the diagnostic-therapeutic network. Category 1 nodes were more frequently linked to etiology and pathogenesis, highlighting their theoretical significance. In contrast, Category 3 nodes exhibited the lowest proportions across all terminology types, reflecting their peripheral status within the network.

Further statistical comparisons of centrality metrics among node categories (Figure S10D) demonstrated that Category 2 nodes significantly outperformed the other categories across all metrics, firmly establishing their status as core nodes within the network. Category 1 nodes showed intermediate importance, while Category 3 nodes scored the lowest on most metrics. This stratification provides a crucial foundation for subsequent extraction of core features across different node categories, supporting a deeper understanding of the hierarchical structure and functional roles within the TCM diagnostic-therapeutic terminology network.

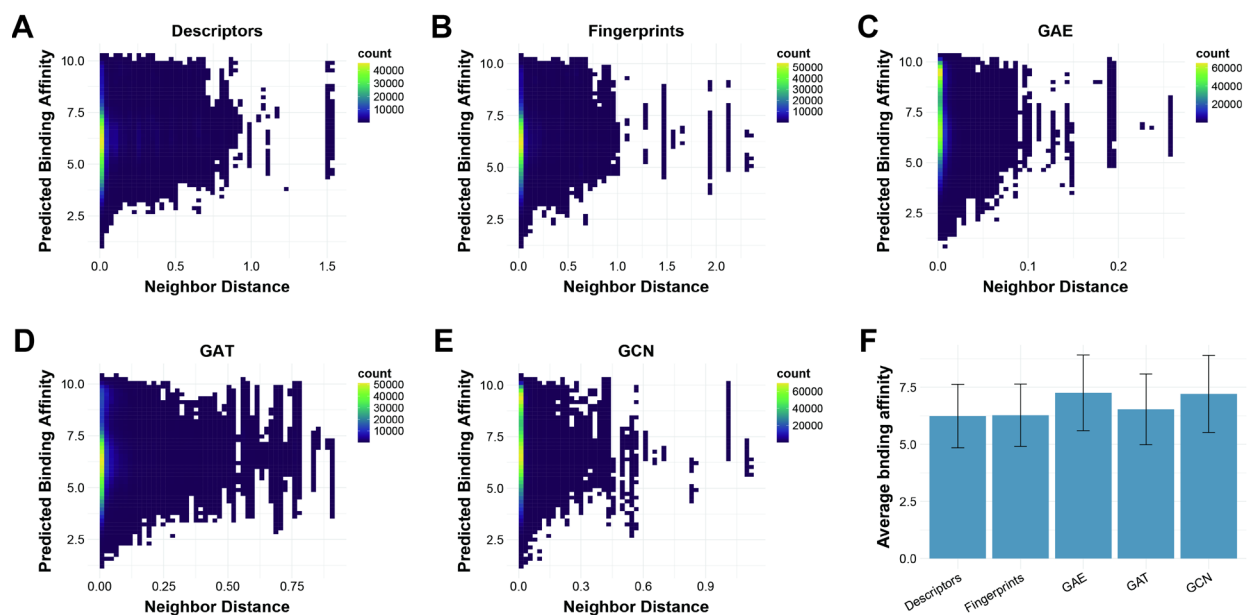


Fig. S1. Relationship between neighbor distance and predicted binding affinity across different feature representation methods. (A) Molecular descriptors (Descriptors). (B) Molecular fingerprints (Fingerprints). (C) Graph autoencoder (GAE). (D) Graph attention network (GAT). (E) Graph convolutional network (GCN). (F) Comparison of average binding affinity at short neighbor distances across different feature representation methods. Error bars represent standard deviations.

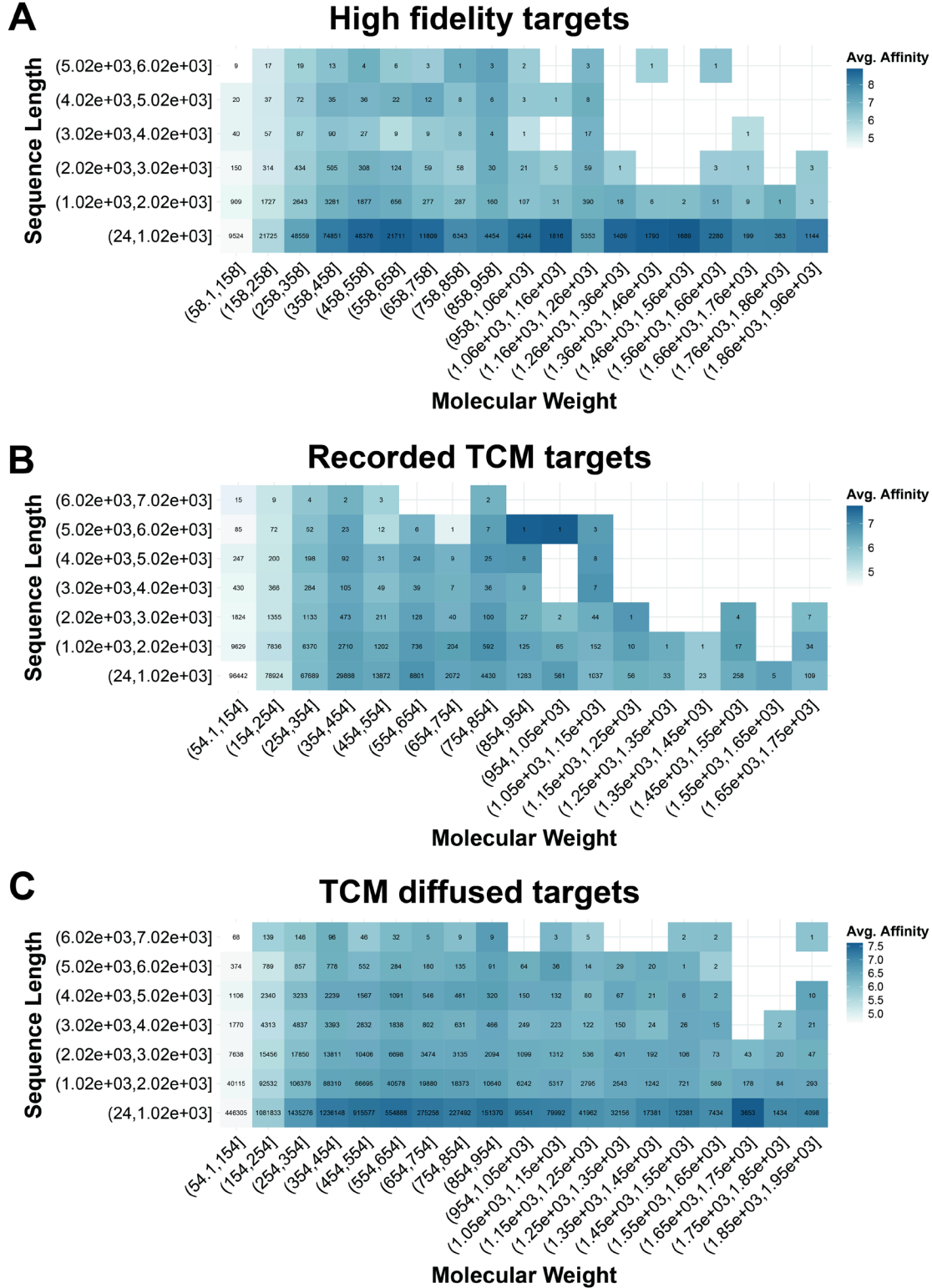


Fig. S2. Heatmap of the effects of molecular weight and target sequence length on binding affinity. Each grid shows the number of samples at that point. (A) High fidelity targets. (B) Recorded TCM targets. (C) TCM diffused targets.

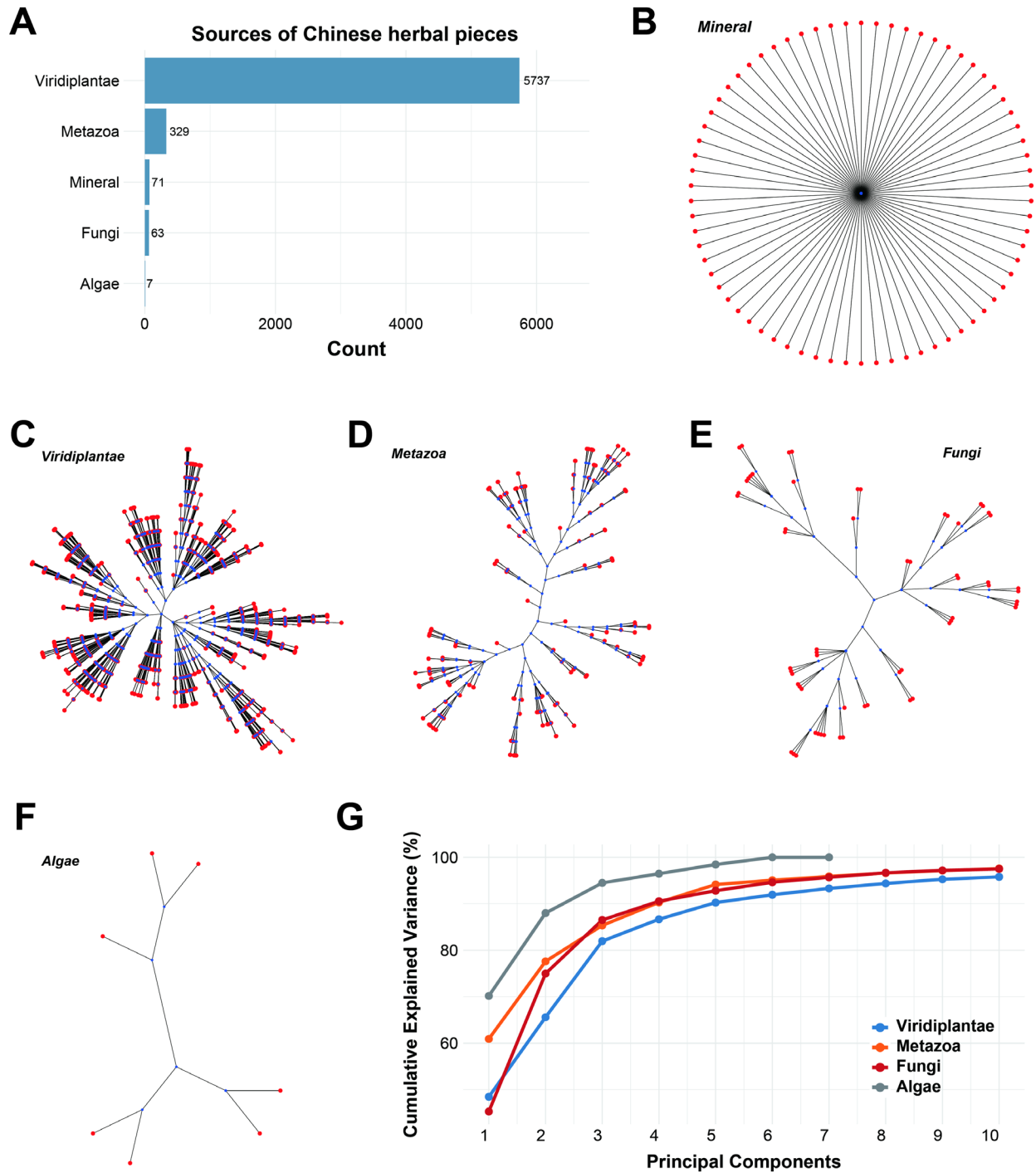


Fig. S3. Classification and phylogenetic analysis of Chinese herbal pieces. (A) Taxonomic distribution of Chinese herbal piece sources. (B–F) Phylogenetic trees of different source categories: (B) Mineral, (C) Viridiplantae, (D) Metazoa, (E) Fungi, and (F) Algae. (G) Principal component analysis (PCA) of source characteristics, showing cumulative explained variance.

Metabolic and circulatory imbalances within the body

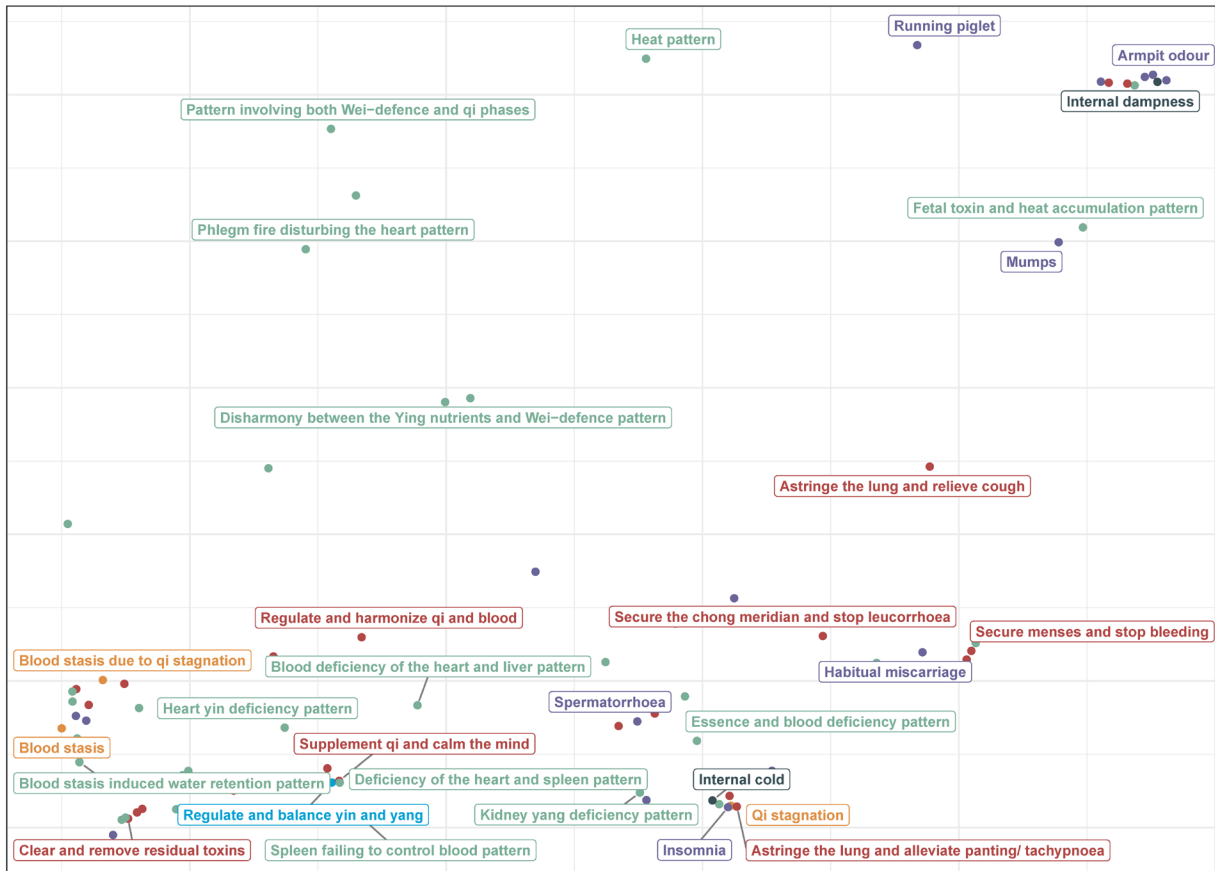


Fig. S4. Metabolic and circulatory imbalances within the body. This category represents conditions resulting from disruptions in metabolism and the circulatory system, characterized by pathologies such as qi stagnation, blood stasis, and internal dampness. Symptoms often include impaired digestion, fluid retention, and imbalances in yin and yang. TCM treatments emphasize warming yang, tonifying qi, and invigorating blood circulation to restore internal metabolic and circulatory harmony.

Organ aging and immune deficiency

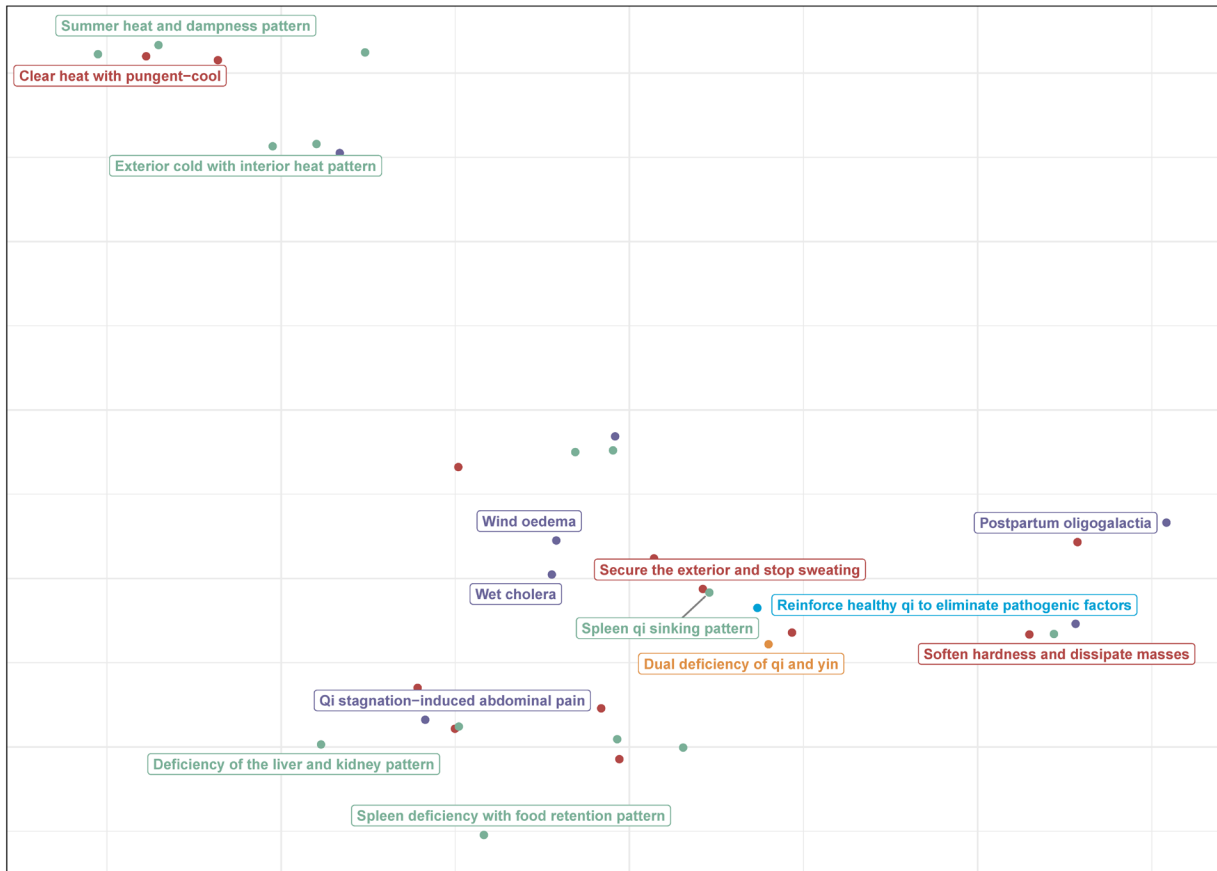


Fig. S5. Organ aging and immune deficiency. This category highlights conditions associated with aging and immune system decline, often presenting as qi deficiency, yin deficiency, and impaired organ function. Common syndromes include kidney yin deficiency, spleen qi sinking, and blood deficiency. TCM treatments focus on tonifying qi and yin, nourishing the kidneys, and enhancing overall immunity to slow organ degeneration and improve resilience.

Influences of lifestyle factors and environmental

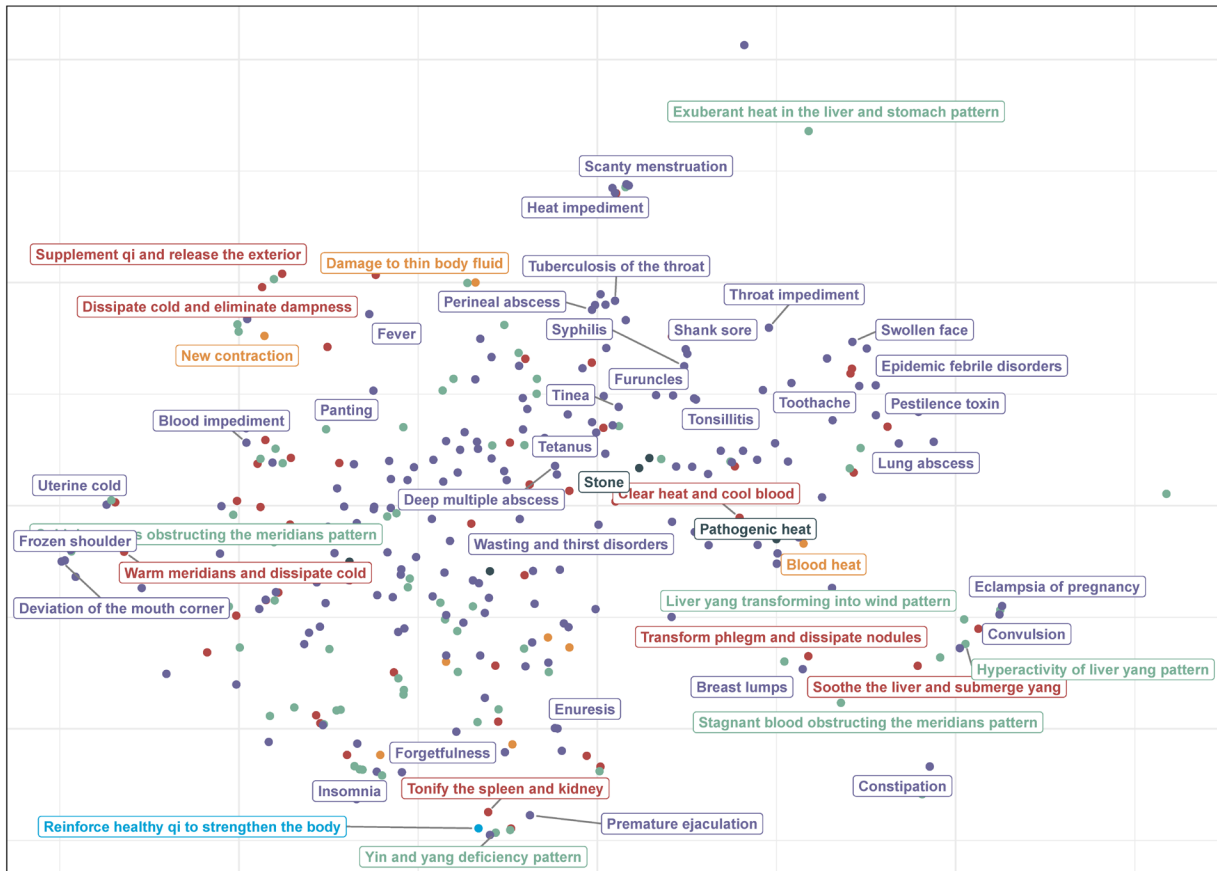


Fig. S6. Influences of lifestyle and environmental conditions. This category addresses the impact of lifestyle choices and environmental factors, including unhealthy diets and exposure to external cold or heat. Pathologies such as qi stagnation, blood heat, and dampness accumulation are common. TCM treatments target clearing heat, removing dampness, and invigorating blood flow to correct imbalances caused by external and lifestyle-related factors.

Physical and mental stress and external stimuli

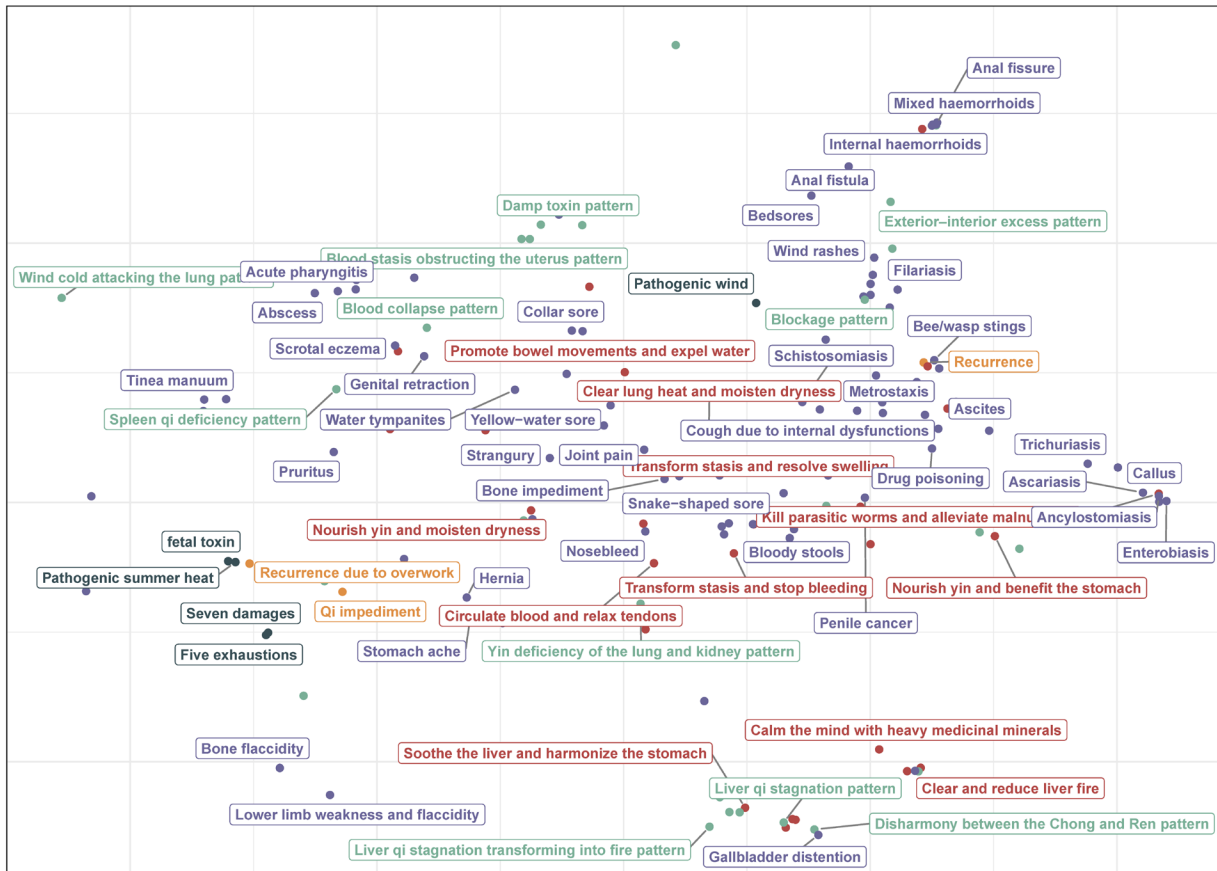


Fig. S7. Physical and mental stress and external stimuli. This category reflects conditions triggered by prolonged stress, overwork, or environmental stimuli, often manifesting as qi stagnation, heat, or wind invasion. Symptoms include insomnia, irritability, and fatigue. TCM treatments emphasize soothing the liver, relieving qi stagnation, and harmonizing the body to alleviate both physical and mental stressors.

Internal pathological changes and infectious factors

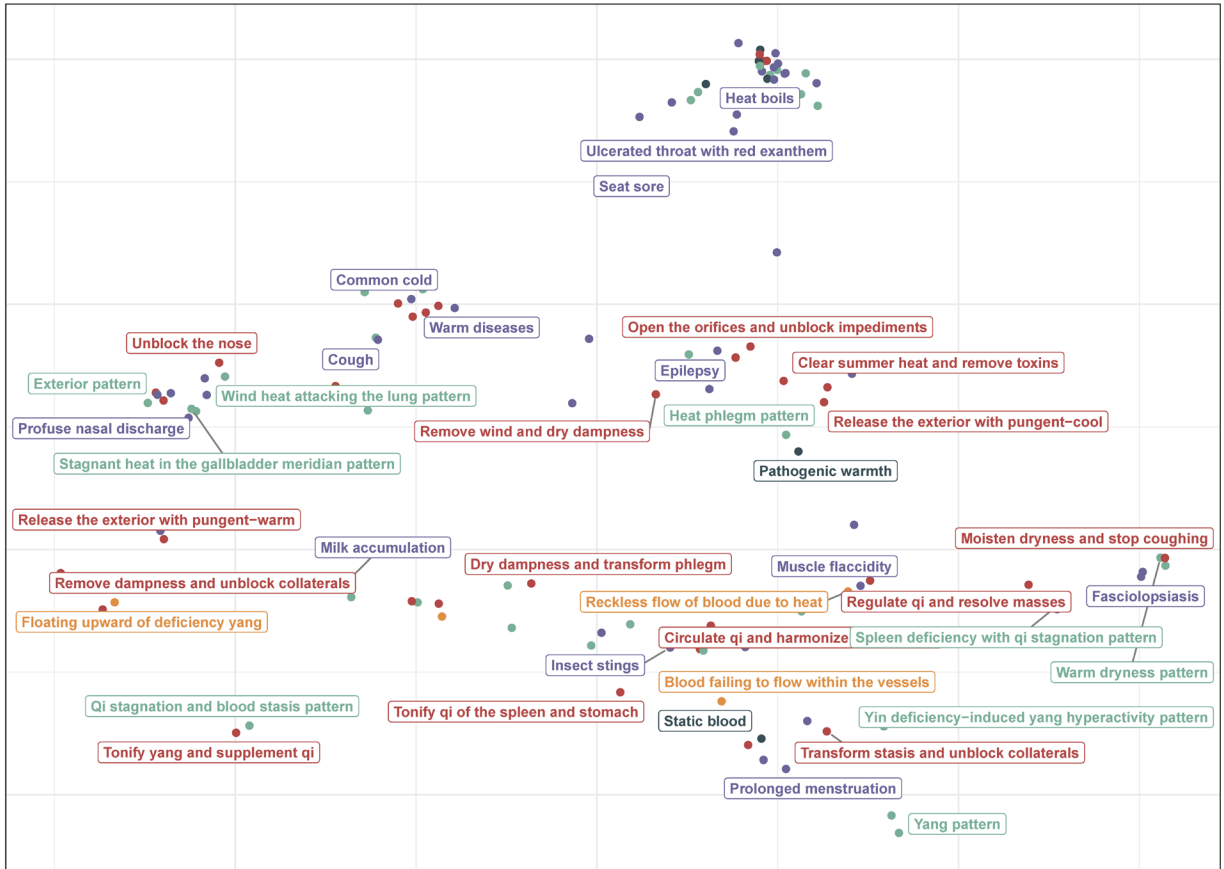


Fig. S8. Internal pathological changes and infectious factors. This category focuses on conditions arising from internal pathological changes and external infections. Key mechanisms include internal wind, blood stasis, and pathogenic warmth. Symptoms may involve heat boils, phlegm patterns, and chronic inflammation. TCM treatments integrate detoxification, clearing heat, and resolving phlegm to manage infections and restore internal balance.

Dry dampness and harmonize the stomach



Fig. S9. Dry dampness and harmonize the stomach. This category, though less prominent, involves conditions linked to spleen and stomach dysfunction caused by dampness or phlegm retention. Symptoms include digestive issues and dampness obstruction. TCM treatments focus on drying dampness and harmonizing the stomach to restore digestive health and systemic balance.

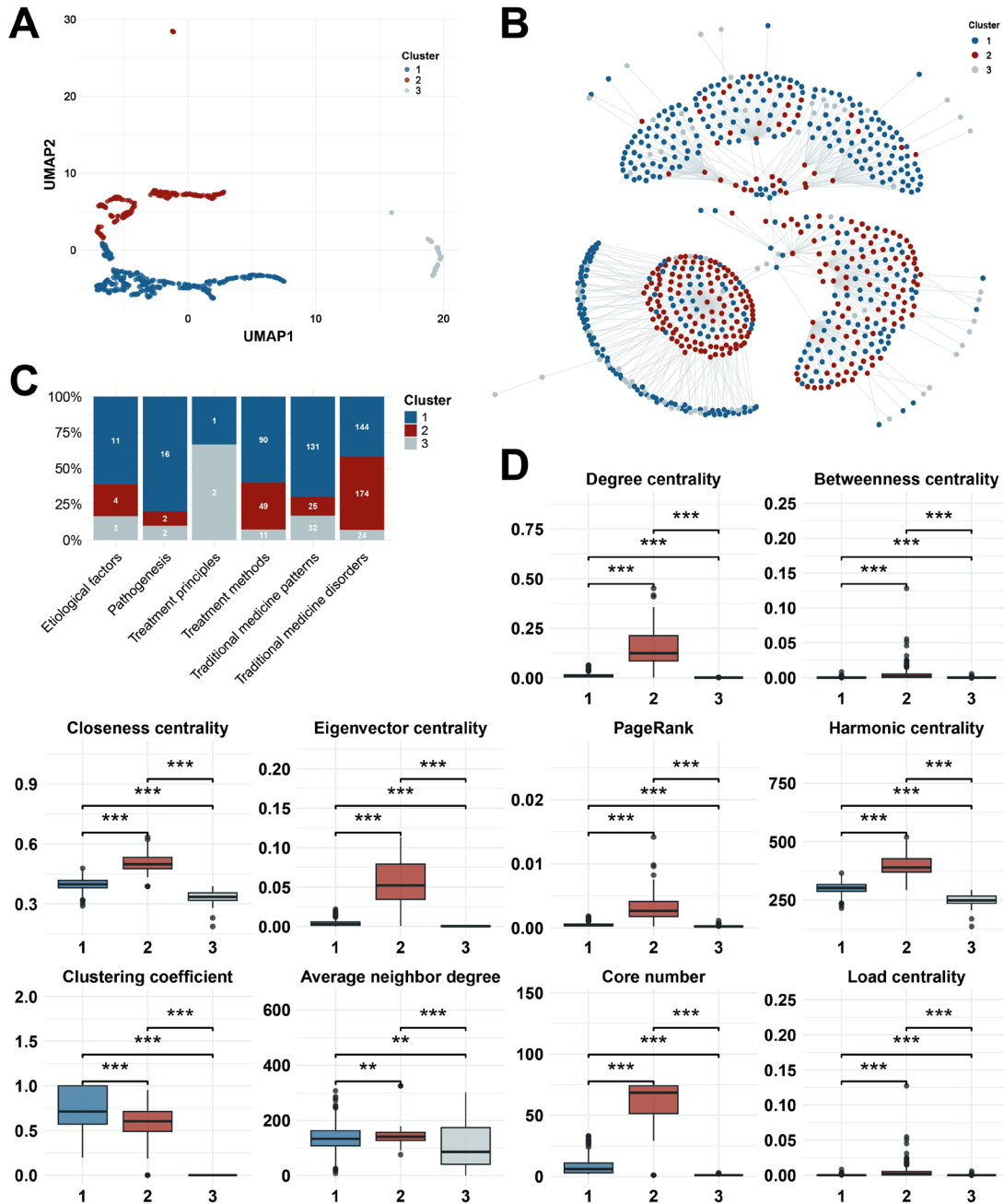


Fig. S10. Core feature analysis of TCM diagnostic terminology. (A) UMAP visualization of node importance based on centrality measures, including degree, betweenness, closeness, eigenvector, PageRank, harmonic, clustering coefficient, average neighbor degree, core number, and load centrality. (B) Network layout of nodes grouped by importance levels derived from centrality measures. (C) Proportional distribution of TCM diagnostic terminologies (etiological factors, pathogenesis, treatment methods, principles, and patterns) across node categories. (D) Centrality metric distributions for node categories, with Category 2 showing the highest centrality and core importance, followed by Category 1, and Category 3 being the least significant. $**P < 0.01$; $***P < 0.001$

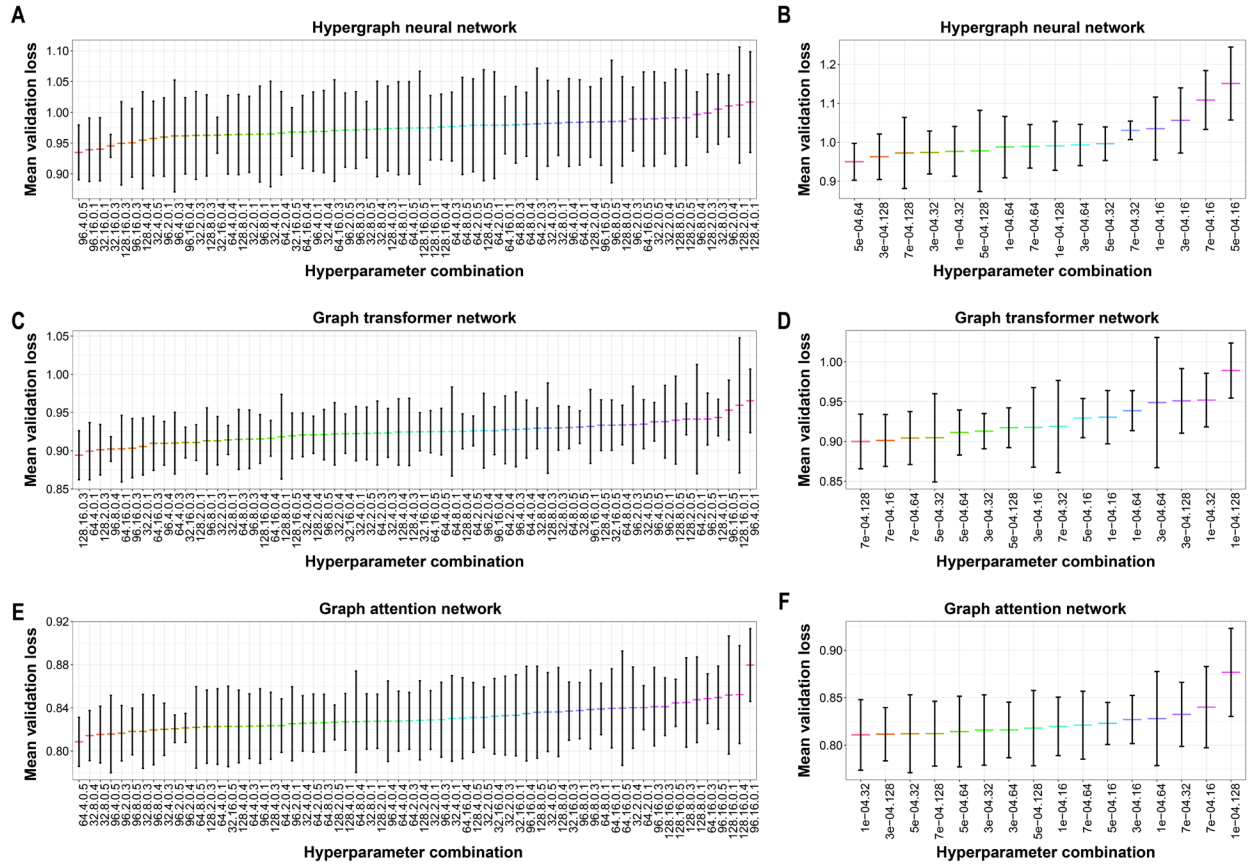


Fig. S11. Hyperparameter optimization of three graph neural network models. (A, B) Hypergraph neural network: Optimization of structural parameters (A) including hidden dimensions (hidden_dim), number of attention heads (num_heads), and dropout rate (dropout_rate), followed by training parameters (B) including learning rate (learning_rate) and batch size (batch_size). (C, D) Graph transformer network: Structural parameter optimization (C) and training parameter optimization (D), with mean validation loss showing the effectiveness of parameter combinations. (E, F) Graph attention network: Two-stage optimization of structural parameters (E) and training parameters (F), evaluated by mean validation loss. A two-stage grid search with 5-fold cross-validation was employed. Structural parameters were optimized first to establish the ideal architecture, followed by refinement of training parameters to stabilize training and enhance generalization, as indicated by reduced mean validation loss.

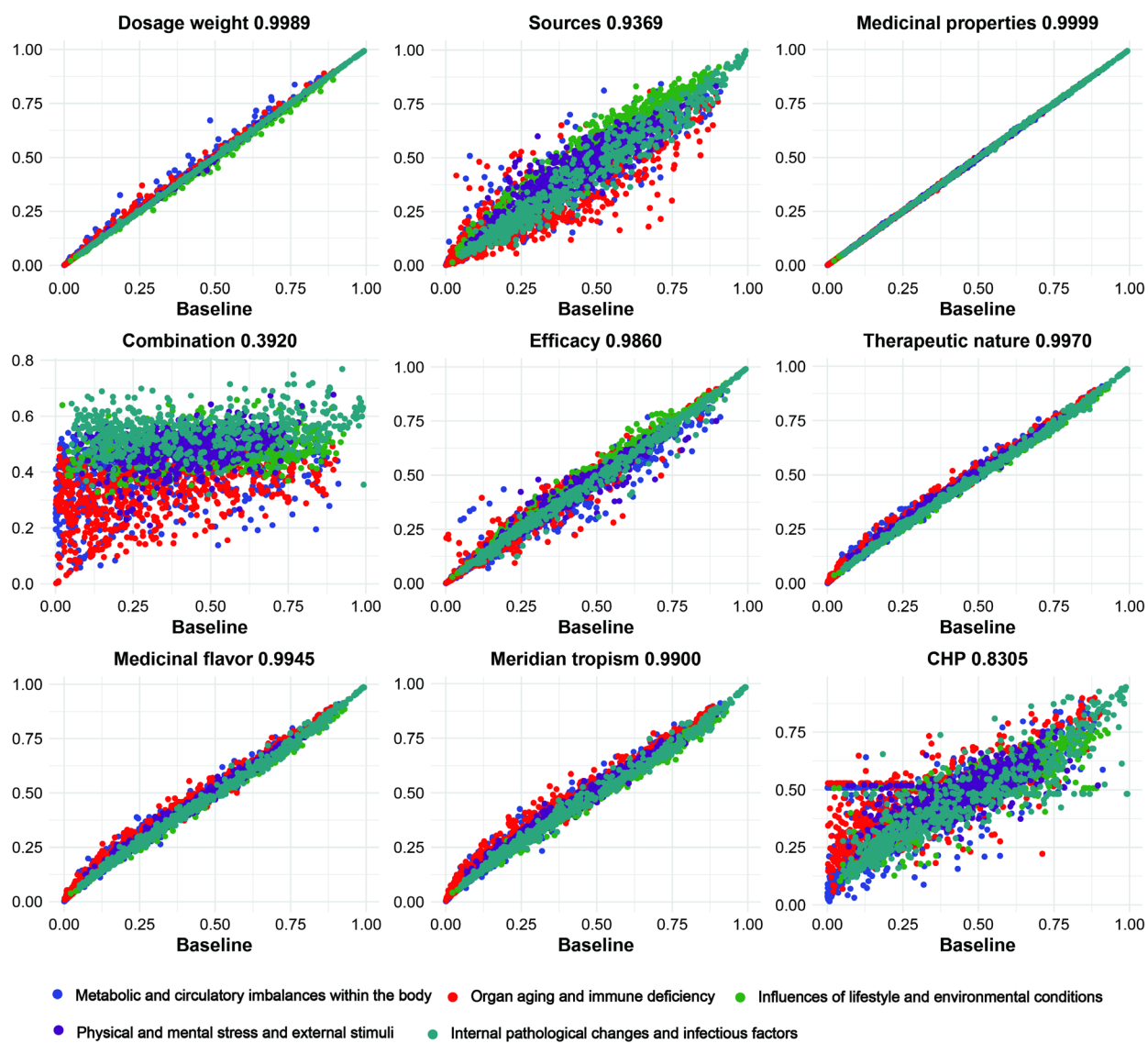


Fig. S12. Analysis of prediction changes before and after feature and node zeroing. Scatter plots illustrate the impact of feature and node zeroing on prediction results compared to the baseline using the graph attention network. Features: Dosage weight, sources, medicinal properties, combination, and efficacy. Nodes: Therapeutic nature, medicinal flavor, meridian tropism, and CHP (Chinese herbal pieces). Correlation coefficients between the zeroed and baseline predictions are indicated for each feature and node. Points are colored by TCM etiological types.

Table S1. Performance comparison of graph neural network models across five major TCM etiological types

Model type	Metrics	Metabolic and circulatory imbalances within the body			Organ aging and immune deficiency			Influences of lifestyle and environmental conditions			Physical and mental stress and external stimuli			Internal pathological changes and infectious factors		
		Cal	Val	Test	Cal	Val	Test	Cal	Val	Test	Cal	Val	Test	Cal	Val	Test
Graph transformer network	Precision	0.166	0.1751	0.1111	0.1313	0.1347	0.1111	0.7082	0.6961	0.7258	0.1606	0.1538	0.1483	0.5665	0.5558	0.5774
	Recall	0.8037	0.8214	0.7692	0.8352	0.8193	0.675	0.772	0.7819	0.7989	0.507	0.5179	0.5167	0.7924	0.7466	0.7806
	F1 Score	0.2752	0.2887	0.1942	0.2269	0.2313	0.1908	0.7387	0.7365	0.7606	0.244	0.2372	0.2305	0.6607	0.6372	0.6638
	AUC	0.8259	0.8445	0.8168	0.7962	0.7852	0.7446	0.733	0.6971	0.7641	0.6672	0.6713	0.6178	0.8336	0.8187	0.8241
	Accuracy	0.7314	0.7218	0.7243	0.6349	0.6301	0.6196	0.687	0.6768	0.7093	0.6826	0.6948	0.6561	0.7521	0.7447	0.7425
Hypergraph neural network	Precision	0.3133	0.2768	0.1947	0.2621	0.2218	0.1655	0.7895	0.7574	0.7578	0.2559	0.1843	0.1961	0.6758	0.6241	0.6301
	Recall	0.9074	0.7381	0.8462	0.8938	0.7349	0.575	0.7368	0.721	0.7011	0.8279	0.6518	0.6667	0.7978	0.7057	0.7041
	F1 Score	0.4658	0.4026	0.3165	0.4053	0.3408	0.257	0.7622	0.7388	0.7284	0.391	0.2874	0.303	0.7318	0.6624	0.6651
	AUC	0.9558	0.8869	0.8994	0.9386	0.8028	0.7766	0.8209	0.7674	0.7841	0.8627	0.7323	0.7317	0.8909	0.8295	0.8445
	Accuracy	0.868	0.8494	0.8422	0.8318	0.8069	0.7791	0.7366	0.7054	0.6977	0.7394	0.7038	0.6944	0.8219	0.784	0.7691
Graph attention network	Specificity	0.8653	0.8576	0.842	0.8275	0.8121	0.7936	0.7364	0.6841	0.6929	0.7295	0.709	0.6974	0.8324	0.8175	0.8005
	Precision	0.2241	0.2207	0.1489	0.2191	0.215	0.1825	0.7465	0.7289	0.7647	0.219	0.1802	0.2113	0.6182	0.6104	0.6203
	Recall	0.8407	0.7857	0.8077	0.7656	0.759	0.625	0.7618	0.7691	0.7471	0.714	0.6518	0.75	0.7809	0.7384	0.75
	F1 Score	0.3539	0.3446	0.2515	0.3407	0.3351	0.2825	0.7541	0.7484	0.7558	0.3352	0.2824	0.3297	0.6901	0.6683	0.679
	AUC	0.9004	0.8842	0.8918	0.8736	0.8347	0.8106	0.7939	0.765	0.8013	0.7757	0.7341	0.7589	0.8644	0.8393	0.8366
	Accuracy	0.8052	0.7946	0.7924	0.8099	0.7954	0.789	0.7152	0.7013	0.7209	0.7138	0.6964	0.696	0.7864	0.7799	0.7691
	Specificity	0.8028	0.7953	0.7917	0.813	0.7981	0.8007	0.6527	0.6085	0.685	0.7138	0.7009	0.69	0.7889	0.7977	0.7783

The dataset comprises 6,080 samples, divided into 4,256 training graphs (Cal), 1,222 validation graphs (Val), and 602 test graphs (Test), following a 7:2:1 split. Positive sample proportions for the five major TCM etiological types are as follows:

Metabolic and circulatory imbalances within the body: Training (6.34%), Validation (6.87%), Test (4.32%);

Organ aging and immune deficiency: Training (6.41%), Validation (6.79%), Test (6.64%);

Influences of lifestyle and environmental conditions: Training (57.31%), Validation (57.77%), Test (57.81%);

Physical and mental stress and external stimuli: Training (10.10%), Validation (9.17%), Test (9.97%);

Internal pathological changes and infectious factors: Training (30.45%), Validation (30.03%), Test (32.56%).

Supplemental Data

Data S1. Overview of TCM-MKG data sources and key information tables.

Data S2. Hyperparameter optimization and evaluation of graph neural network models for Chinese herbal formulas classification.

Data S3. Feature and node contribution analysis using zeroing method.

Data S4. Chinese herbal formulas for COVID-19 management: collection and composition.

Data S5. Model prediction results and attention weights for Chinese herbal formulas in COVID-19 management.

Data S6. Analysis of frequency and attention weights of Chinese herbal pieces and herb pairs in COVID-19 formulas.

Data S7. Component-target network for Radix Astragali and associated KEGG pathways

References

- [1] Zeng, J., & Jia, X. (2024). Systems Theory-Driven Framework for AI Integration into the Holistic Material Basis Research of Traditional Chinese Medicine. *Engineering*, 40, 28-50. <https://doi.org/10.1016/j.eng.2024.04.009>
- [2] Shen, X., & Yin, F. (2021). The mechanisms and clinical application of Traditional Chinese Medicine Lianhua-Qingwen capsule. *Biomedicine & Pharmacotherapy*, 142, 111998. <https://doi.org/10.1016/j.biopha.2021.111998>
- [3] Xing, D., & Liu, Z. (2021). Effectiveness and Safety of Traditional Chinese Medicine in Treating COVID-19: Clinical Evidence from China. *Aging and disease*, 12(8), 1850–1856. <https://doi.org/10.14336/AD.2021.0906>
- [4] Chu E. (2018). Wedding Rigorous Scientific Methodology and Ancient Herbal Wisdom to Benefit Cancer Patients: The Development of PHY906. *Oncology (Williston Park, N.Y.)*, 32(2), e20–e27.
- [5] Wang, Y., Shi, X., Li, L., Efferth, T., & Shang, D. (2021). The Impact of Artificial Intelligence on Traditional Chinese Medicine. *The American journal of Chinese medicine*, 49(6), 1297–1314. <https://doi.org/10.1142/S0192415X21500622>
- [6] Zhang, S., Wang, W., Pi, X., He, Z., & Liu, H. (2023). Advances in the Application of Traditional Chinese Medicine Using Artificial Intelligence: A Review. *The American journal of Chinese medicine*, 51(5), 1067–1083. <https://doi.org/10.1142/S0192415X23500490>
- [7] Chu, X., Sun, B., Huang, Q., Peng, S., Zhou, Y., & Zhang, Y. (2020). Quantitative knowledge presentation models of traditional Chinese medicine (TCM): A review. *Artificial intelligence in medicine*, 103, 101810. <https://doi.org/10.1016/j.artmed.2020.101810>
- [8] Gan, X., Shu, Z., Wang, X., Yan, D., Li, J., Ofaim, S., Albert, R., Li, X., Liu, B., Zhou, X., & Barabási, L. (2023). Network medicine framework reveals generic herb-symptom effectiveness of traditional Chinese medicine. *Science Advances*. <https://doi.org/adh0215>
- [9] Pan, D., Guo, Y., Fan, Y., & Wan, H. (2024). Development and Application of Traditional Chinese Medicine Using AI Machine Learning and Deep Learning Strategies. *The American journal of Chinese medicine*, 52(3), 605–623. <https://doi.org/10.1142/S0192415X24500265>
- [10] Johnson, R., Li, M. M., Noori, A., Queen, O., & Zitnik, M. (2024). Graph Artificial Intelligence in Medicine. *Annual review of biomedical data science*, 7(1), 345–368. <https://doi.org/10.1146/annurev-biodatasci-110723-024625>
- [11] Zeng, X., Tu, X., Liu, Y., Fu, X., & Su, Y. (2022). Toward better drug discovery with knowledge graph. *Current Opinion in Structural Biology*, 72, 114-126. <https://doi.org/10.1016/j.sbi.2021.09.003>
- [12] Zhou, W., Yang, K., Zeng, J., Lai, X., Wang, X., Ji, C., Li, Y., Zhang, P., & Li, S. (2021). FordNet: Recommending traditional Chinese medicine formula via deep neural network integrating phenotype and molecule. *Pharmacological research*, 173, 105752. <https://doi.org/10.1016/j.phrs.2021.105752>
- [13] Zhang, H., Zhang, J., Ni, W., Jiang, Y., Liu, K., Sun, D., & Li, J. (2022). Transformer- and Generative Adversarial Network-Based Inpatient Traditional Chinese Medicine Prescription Recommendation: Development Study. *JMIR medical informatics*, 10(5), e35239. <https://doi.org/10.2196/35239>
- [14] Yang, K., Dong, X., Zhang, S., Yu, H., Zhong, L., Zhang, L., Zhao, H., Hou, Y., Song, X., & Zhou, X. (2024). PresRecRF: Herbal prescription recommendation via the representation fusion of large TCM semantics and molecular knowledge. *Phytomedicine*, 135, 156116. <https://doi.org/10.1016/j.phymed.2024.156116>
- [15] Koh, H. Y., Nguyen, A. T., Pan, S., May, L. T., & Webb, G. I. (2024). Physicochemical graph neural network for learning protein–ligand interaction fingerprints from sequence data. *Nature Machine Intelligence*, 6(6), 673-687. <https://doi.org/10.1038/s42256-024-00847-1>.
- [16] Wang, X., Cheng, Y., Yang, Y., Yu, Y., Li, F., & Peng, S. (2023). Multitask joint strategies of self-supervised representation learning on biomedical networks for drug discovery. *Nature Machine Intelligence*, 5(4), 445-456. <https://doi.org/10.1038/s42256-023-00640-6>
- [17] Xu, H., Li, S., Liu, J., Cheng, J., Kang, L., Li, W., Zhong, Y., Wei, C., Fu, L., Qi, J., Zhang, Y., You, M., Zhou, Z., Zhang, C., Su, H., Yao, S., Zhou, Z., Shi, Y., Deng, R., Lv, Q., ... Huang, L. (2023). Bioactive compounds from Huashi Baidu decoction possess both antiviral and anti-inflammatory effects against COVID-19. *Proceedings of the National Academy of Sciences of the United States of America*, 120(18), e2301775120. <https://doi.org/10.1073/pnas.2301775120>
- [18] Huang, L., Qin, W., Guo, Z., Li, X., Li, F., & Wang, X. (2023). Application of weighted gene co-expression network and immune infiltration for explorations of key genes in the brain of elderly COVID-19 patients. *Frontiers in immunology*, 14, 1157179. <https://doi.org/10.3389/fimmu.2023.1157179>
- [19] Bédard-Matteau, J., Soulé, A., Liu, K. Y., Fourcade, L., Fraser, D. D., Emad, A., & Rousseau, S. (2024). Circulating IL-17F, but not IL-17A, is elevated in severe COVID-19 and leads to an ERK1/2 and p38 MAPK-dependent increase in ICAM-1 cell surface expression and neutrophil adhesion on endothelial cells. *Frontiers in immunology*, 15, 1452788. <https://doi.org/10.3389/fimmu.2024.1452788>

- [20] Berta, B., Tordai, H., Lukács, G. L., Papp, B., Enyedi, Á., Padányi, R., & Hegedűs, T. (2024). SARS-CoV-2 envelope protein alters calcium signaling via SERCA interactions. *Scientific reports*, 14(1), 21200. <https://doi.org/10.1038/s41598-024-71144-5>
- [21] Zhang, H., Zhang, J., Ni, W., Jiang, Y., Liu, K., Sun, D., & Li, J. (2022). Transformer- and Generative Adversarial Network-Based Inpatient Traditional Chinese Medicine Prescription Recommendation: Development Study. *JMIR medical informatics*, 10(5), e35239. <https://doi.org/10.2196/35239>
- [22] Lin, Y., Huang, W., Ou, S., Hung, H., Cheng, W., Lin, S., Lin, H., & Huang, S. (2019). Neural network analysis of Chinese herbal medicine prescriptions for patients with colorectal cancer. *Complementary Therapies in Medicine*, 42, 279-285. <https://doi.org/10.1016/j.ctim.2018.12.001>
- [23] Zhou, W., Yang, K., Zeng, J., Lai, X., Wang, X., Ji, C., Li, Y., Zhang, P., & Li, S. (2021). FordNet: Recommending traditional Chinese medicine formula via deep neural network integrating phenotype and molecule. *Pharmacological research*, 173, 105752. <https://doi.org/10.1016/j.phrs.2021.105752>
- [24] Yang, K., Dong, X., Zhang, S., Yu, H., Zhong, L., Zhang, L., Zhao, H., Hou, Y., Song, X., & Zhou, X. (2024). PresRecRF: Herbal prescription recommendation via the representation fusion of large TCM semantics and molecular knowledge. *Phytomedicine*, 135, 156116. <https://doi.org/10.1016/j.phymed.2024.156116>
- [25] R. Antar, A. A., & Cox, A. L. (2024). Translating insights into therapies for Long Covid. *Science Translational Medicine*. <https://doi.org/ado2106>
- [26] Coordinators, N. R. (2016). Database resources of the National Center for Biotechnology Information. *Nucleic Acids Research*, 44(D1), D7-D19. <https://doi.org/10.1093/nar/gkv1290>
- [27] Huang, L., Xie, D., Yu, Y., Liu, H., Shi, Y., Shi, T., & Wen, C. (2018). TCMID 2.0: a comprehensive resource for TCM. *Nucleic acids research*, 46(D1), D1117–D1120. <https://doi.org/10.1093/nar/gkx1028>
- [28] Lv, Q., Chen, G., He, H., Yang, Z., Zhao, L., Chen, H. Y., & Chen, C. Y. (2023). TCMBank: bridges between the largest herbal medicines, chemical ingredients, target proteins, and associated diseases with intelligence text mining. *Chemical science*, 14(39), 10684–10701. <https://doi.org/10.1039/d3sc02139d>
- [29] Wu, Y., Zhang, F., Yang, K., Fang, S., Bu, D., Li, H., Sun, L., Hu, H., Gao, K., Wang, W., Zhou, X., Zhao, Y., & Chen, J. (2019). SymMap: an integrative database of traditional Chinese medicine enhanced by symptom mapping. *Nucleic acids research*, 47(D1), D1110–D1117. <https://doi.org/10.1093/nar/gky1021>
- [30] Yan, D., Zheng, G., Wang, C., Chen, Z., Mao, T., Gao, J., Yan, Y., Chen, X., Ji, X., Yu, J., Mo, S., Wen, H., Han, W., Zhou, M., Wang, Y., Wang, J., Tang, K., & Cao, Z. (2022). HIT 2.0: an enhanced platform for Herbal Ingredients' Targets. *Nucleic acids research*, 50(D1), D1238–D1243. <https://doi.org/10.1093/nar/gkab1011>
- [31] Fang, S., Dong, L., Liu, L., Guo, J., Zhao, L., Zhang, J., Bu, D., Liu, X., Huo, P., Cao, W., Dong, Q., Wu, J., Zeng, X., Wu, Y., & Zhao, Y. (2021). HERB: a high-throughput experiment- and reference-guided database of traditional Chinese medicine. *Nucleic acids research*, 49(D1), D1197–D1206. <https://doi.org/10.1093/nar/gkaa1063>
- [32] Zhang, Y., Li, X., Shi, Y., Chen, T., Xu, Z., Wang, P., Yu, M., Chen, W., Li, B., Jing, Z., Jiang, H., Fu, L., Gao, W., Jiang, Y., Du, X., Gong, Z., Zhu, W., Yang, H., & Xu, H. (2023). ETCM v2.0: An update with comprehensive resource and rich annotations for traditional Chinese medicine. *Acta pharmaceutica Sinica. B*, 13(6), 2559–2571. <https://doi.org/10.1016/j.apsb.2023.03.012>
- [33] Ru, J., Li, P., Wang, J., Zhou, W., Li, B., Huang, C., Li, P., Guo, Z., Tao, W., Yang, Y., Xu, X., Li, Y., Wang, Y., & Yang, L. (2014). TCMSP: a database of systems pharmacology for drug discovery from herbal medicines. *Journal of cheminformatics*, 6, 13. <https://doi.org/10.1186/1758-2946-6-13>
- [34] Hou, D., Lin, H., Feng, Y., Zhou, K., Li, X., Yang, Y., Wang, S., Yang, X., Wang, J., Zhao, H., Zhang, X., Fan, J., Lu, S., Wang, D., Zhu, L., Ju, D., Chen, Y. Z., & Zeng, X. (2024). CMAUP database update 2024: extended functional and association information of useful plants for biomedical research. *Nucleic acids research*, 52(D1), D1508–D1518. <https://doi.org/10.1093/nar/gkad921>
- [35] Kim, H. W., Wang, M., Leber, C. A., Nothias, L. F., Reher, R., Kang, K. B., van der Hoof, J. J. J., Dorrestein, P. C., Gerwick, W. H., & Cottrell, G. W. (2021). NPClassifier: A Deep Neural Network-Based Structural Classification Tool for Natural Products. *Journal of natural products*, 84(11), 2795–2807. <https://doi.org/10.1021/acs.jnatprod.1c00399>
- [36] Wishart, D. S., Feunang, Y. D., Guo, A. C., Lo, E. J., Marcu, A., Grant, J. R., Sajed, T., Johnson, D., Li, C., Sayeeda, Z., Assempour, N., Iynkkaran, I., Liu, Y., Maciejewski, A., Gale, N., Wilson, A., Chin, L., Cummings, R., Le, D., Pon, A., ... Wilson, M. (2018). DrugBank 5.0: a major update to the DrugBank database for 2018. *Nucleic acids research*, 46(D1), D1074–D1082. <https://doi.org/10.1093/nar/gkx1037>
- [37] Zhou, Y., Zhang, Y., Zhao, D., Yu, X., Shen, X., Zhou, Y., Wang, S., Qiu, Y., Chen, Y., & Zhu, F. (2024). TTD: Therapeutic Target Database describing target druggability information. *Nucleic acids research*, 52(D1), D1465–D1477. <https://doi.org/10.1093/nar/gkad751>

- [38] Szklarczyk, D., Santos, A., von Mering, C., Jensen, L. J., Bork, P., & Kuhn, M. (2016). STITCH 5: augmenting protein-chemical interaction networks with tissue and affinity data. *Nucleic acids research*, 44(D1), D380–D384. <https://doi.org/10.1093/nar/gkv1277>
- [39] Gilson, M. K., Liu, T., Baitaluk, M., Nicola, G., Hwang, L., & Chong, J. (2016). BindingDB in 2015: A public database for medicinal chemistry, computational chemistry and systems pharmacology. *Nucleic acids research*, 44(D1), D1045–D1053. <https://doi.org/10.1093/nar/gkv1072>
- [40] Martin, F. J., Amode, M. R., Aneja, A., Azov, A. G., Barnes, I., Becker, A., Bennett, R., Berry, A., Bhai, J., Bhurji, S. K., Bignell, A., Boddu, S., Branco Lins, P. R., Brooks, L., Ramaraju, S. B., Charkhchi, M., Cockburn, A., Davidson, C., Dodiya, K., . . . Flicek, P. (2023). Ensembl 2023. *Nucleic Acids Research*, 51(D1), D933–D941. <https://doi.org/10.1093/nar/gkac958>
- [41] Consortium, T. U., Bateman, A., Martin, M., Orchard, S., Magrane, M., Ahmad, S., Alpi, E., H, E., Britto, R., Cukura, A., Denny, P., Dogan, T., Ebenezer, T., Fan, J., Garmiri, P., Jose, L., Hussein, A., Ignatchenko, A., Insana, G., . . . Zhang, J. (2023). UniProt: The Universal Protein Knowledgebase in 2023. *Nucleic Acids Research*, 51(D1), D523–D531. <https://doi.org/10.1093/nar/gkac1052>
- [42] Szklarczyk, D., Kirsch, R., Koutrouli, M., Nastou, K., Mehryary, F., Hachilif, R., Gable, A. L., Fang, T., Doncheva, N. T., Pyysalo, S., Bork, P., Jensen, L. J., & von Mering, C. (2023). The STRING database in 2023: protein-protein association networks and functional enrichment analyses for any sequenced genome of interest. *Nucleic acids research*, 51(D1), D638–D646. <https://doi.org/10.1093/nar/gkac1000>
- [43] Lo Surdo, P., Iannuccelli, M., Contino, S., Castagnoli, L., Licata, L., Cesareni, G., & Perfetto, L. (2023). SIGNOR 3.0, the SIGnaling network open resource 3.0: 2022 update. *Nucleic acids research*, 51(D1), D631–D637. <https://doi.org/10.1093/nar/gkac883>
- [44] Licata, L., Briganti, L., Peluso, D., Perfetto, L., Iannuccelli, M., Galeota, E., Sacco, F., Palma, A., Nardoza, A. P., Santonico, E., Castagnoli, L., & Cesareni, G. (2012). MINT, the molecular interaction database: 2012 update. *Nucleic acids research*, 40(Database issue), D857–D861. <https://doi.org/10.1093/nar/gkr930>
- [45] Del Toro, N., Shrivastava, A., Ragueneau, E., Meldal, B., Combe, C., Barrera, E., Perfetto, L., How, K., Ratan, P., Shirodkar, G., Lu, O., Mészáros, B., Watkins, X., Pundir, S., Licata, L., Iannuccelli, M., Pellegrini, M., Martin, M. J., Panni, S., Duesbury, M., . . . Hermjakob, H. (2022). The IntAct database: efficient access to fine-grained molecular interaction data. *Nucleic acids research*, 50(D1), D648–D653. <https://doi.org/10.1093/nar/gkab1006>
- [46] Stark, C., Breitkreutz, B. J., Reguly, T., Boucher, L., Breitkreutz, A., & Tyers, M. (2006). BioGRID: a general repository for interaction datasets. *Nucleic acids research*, 34(Database issue), D535–D539. <https://doi.org/10.1093/nar/gkj109>
- [47] Bodenreider, O. (2003). The Unified Medical Language System (UMLS): Integrating biomedical terminology. *Nucleic Acids Research*, 32(suppl_1), D267–D270. <https://doi.org/10.1093/nar/gkh061>
- [48] Baron, J. A., Johnson, C. S., Schor, M. A., Olley, D., Nickel, L., Felix, V., Munro, J. B., Bello, S. M., Bearer, C., Lichenstein, R., Bisordi, K., Koka, R., Greene, C., & Schriml, L. M. (2024). The DO-KB Knowledgebase: a 20-year journey developing the disease open science ecosystem. *Nucleic acids research*, 52(D1), D1305–D1314. <https://doi.org/10.1093/nar/gkad1051>
- [49] Piñero, J., Saüch, J., Sanz, F., & Furlong, L. I. (2021). The DisGeNET cytoscape app: Exploring and visualizing disease genomics data. *Computational and structural biotechnology journal*, 19, 2960–2967. <https://doi.org/10.1016/j.csbj.2021.05.015>
- [50] Davis, A. P., Wieggers, T. C., Wieggers, J., Wyatt, B., Johnson, R. J., Sciaky, D., Barkalow, F., Strong, M., Planchart, A., & Mattingly, C. J. (2023). CTD tetramers: a new online tool that computationally links curated chemicals, genes, phenotypes, and diseases to inform molecular mechanisms for environmental health. *Toxicological sciences : an official journal of the Society of Toxicology*, 195(2), 155–168. <https://doi.org/10.1093/toxsci/kfad069>
- [51] Grissa, D., Junge, A., Oprea, T. I., & Jensen, L. J. (2022). Diseases 2.0: a weekly updated database of disease-gene associations from text mining and data integration. *Database : the journal of biological databases and curation*, 2022, baac019. <https://doi.org/10.1093/database/baac019>